A Microfabricated Platform for Controlled Drug Release from Conductive Polymer Thin Films

Karley Benoff

A thesis

submitted in partial fulfillment of the

requirements for the degree of

Master of Science

University of Washington

2020

Committee:

Rajiv Saigal
Alberto Aliseda
Nathan Sniadecki

Program Authorized to Offer Degree:

Mechanical Engineering

University of Washington

Abstract

A Microfabricated Platform for Controlled Drug Release from Conductive Polymer Thin Films

Karley Benoff

Co-Chairs of the Supervisory Committee:

Rajiv Saigal, MD Ph.D.
Assistant Professor
Neurological Surgery

Alberto Aliseda, Ph.D.
PACCAR Endowed Professor
Mechanical Engineering

There is great interest in exploring multimodal strategies for the treatment of spinal cord injury (SCI). In animal models of SCI, multimodal treatments combine targeted drug delivery, using the experimental drug, quipazine, with therapeutic stimulation to improve functional movement. However, there is currently a sparse number of devices to elucidate treatment efficacy and an even smaller number of designs appropriate for eventual clinical translation. This research proposes a novel method of delivering quipazine using conductive polymer thin films. Capable of delivering stimulation and locally delivering drug, the biocompatible polymer, polypyrrole (PPy), has been studied for neurological use. In this thesis, we present a microfabricated platform centered around a multielectrode array (MEA) to facilitate preliminary studies on controlled release of quipazine

from PPy. Each MEA facilitated the deposition of eight independent PPy-quipazine films and the simultaneous release of quipazine driven by an applied potential. Quipazine concentrations were calculated using a custom high-performance liquid chromatography (HPLC) method coupled with mass spectrometry (MS). PPy-quipazine film topography and morphology were also examined to shed light on film quality. Although the data and experimental methods contained within this document focus on the delivery of the model drug, quipazine, from PPy, the microfabricated platform can be translated to study various drug dopant and conductive polymer combinations.

TABLE OF CONTENTS

List of Figures iv

List of Tables vi

Chapter 1. Introduction 1

1.1 Project Motivation 1

1.1 Thesis Aims and Organization 2

Chapter 2. Literature Survey on Microfabrication & Techniques in Drug Delivery 3

2.1 Introduction 3

2.2 Spinal Cord Injury and Treatment 3

2.2.1 Electrical Stimulation for Rehabilitation 4

2.3 The Role of Microfabrication in Controlled Drug Delivery 5

2.3.1 Microfabricated Devices 6

2.3.2 Techniques of Microfabrication 6

2.3.3 Advancing Electrode Materials 8

2.4 Delivery of The Experimental Drug, Quipazine 9

2.4.1 A Multimodal Device for Chronic SCI 9

2.4.2 The Barriers of Quipazine 10

2.5 Quantifying Drug Delivery 11

2.5.1 Ultraviolet-visible Absorption (UV-vis) Spectroscopy 11

2.5.2 Mass Spectrometry 12

2.6 Conductive Polymers 13

2.6.1 Polypyrrole 14
2.6.2 A Chamber Device to Manufacture and Test PPy 17
Chapter 3. A Microfabricated Platform for Controlled Drug Release from Polypyrrole 19
3.1 Chapter Overview 19
3.2 The Design and Manufacturing of a Multielectrode Array 19
3.2.1 A novel design 20
3.2.2 Microfabrication 21
3.2.3 Lessons learned in manufacturing 23
3.3 Electrochemical Manufacturing of PPy Films 24
3.3.1 Experimental protocol for film deposition 26
3.3.2 Theoretical film size 27
3.3.3 Film Topography 28
3.3.4 Film Morphology 30
3.4 Discussion and Reflection 32
Chapter 4. Quantifying the Controlled Release of Quipazine from PPy 33
4.1 Introduction 33
4.1.1 Controlled release protocol 33
4.2 UV-vis Spectroscopy 34
4.2.1 Experimental methods: Direct Current 35
4.2.2 Results 35
4.3 Mass Spectrometry 36
4.3.1 Implementing an internal standard 37

4.3.2 Calculating quipazine concentrations 37
4.3.3 Sample preparation and filtering 38
4.3.4 Proof-of-Concept Measurements of Released Quipazine 39
4.3.5 Experimental Methods: Cyclic Voltammetry 40
4.3.6 CV Results 41
4.3.7 Experimental Methods: Passive Release 42
4.3.8 Passive Release Results 43
Chapter 5. Conclusions and Future Directions 44
5.1 Future Directions 44
5.2 Closing Remarks 45
References 46
Appendix A 51

LIST OF FIGURES

Figure 2.1 – (left) dispensing photoresist via a syringe onto a quartz substrate, (right) closing the lid of an automatic spin coater to evenly spread the photoresist..... 7

Figure 2.2 – Substrate held by a gloved researcher after the deposition of gold, highlighting the photopolymerized design visible at the center 8

Figure 2.3 – Example total ion chromatogram produced using methods found in Chapter 4 13

Figure 2.4 – Schematic of conductive polymer states, (a) passive electrolyte solution (b) oxidized film and (c) reduced film with released dopants..... 14

*Figure 2.5 – The polypyrrole cell chamber with an ITO slide covered in dark polypyrrole*17

Figure 3.1 - The microfabricated electrode array design with 8 parallel electrode cells and a simulated PPy film for reference 21

Figure 3.2 – A schematic of the main MEA microfabrication processes, (a) preparing the wafer surface with HMDS (b) applying photoresist (c) exposing a single array design (d) depositing titanium (e) depositing gold (f) dicing of the final array with feature inset of a single electrode 22

Figure 3.3 – Experimental chamber with two polycarbonate plates, a PDMS insert, and a MEA creating 8 independent wells 24

Figure 3.4 – The PDMS curing mold, with 3D printed side walls, an aluminum base, threaded sites for 8 fasteners, and one shoulder screw in place for example 25

Figure 3.5 – Side view of the experimental chamber prior to electrodeposition (left) and after film deposition (right) 27

Figure 3.6 – Topographical image of a film deposited at 108 mC after undergoing cyclic voltammetry experimental conditions (scale bar is 1 mm) 29

Figure 3.7 – Average thicknesses of thin films by deposition charge after experimental release conditions..... 30

Figure 3.8 – SEM image of the center of a PPy film (deposition charge 108 mC) after undergoing cyclic voltammetry experimental conditions (scale bar is 10 µm)..... 31

Figure 3.9 – SEM image a PPy film (deposition charge 108 mC) with arrows highlighting the outermost edge of the film (scale bar is 50 µm)..... 31
Figure 4.1 – Absorbance values obtained using UV-vis spectroscopy with known concentrations of quipazine dissolved in PBS (A) at wavelengths 230 to 390 nm, and (B) at the peak absorbance wavelength of 340 nm..... 34
Figure 4.2 – Average quipazine release (n=4) with standard deviations as measured via UV-vis spectroscopy at 340 nm..... 36
Figure 4.3 – Schematic of how data was extracted, starting from the spiking of MK-212, the internal standard, into the sample vial, the sample entering into the HPLC-MS system, producing a chromatogram, and then calculating the PAR 38
Figure 4.4 – Comparison of filtered and unfiltered samples with known quipazine concentrations plotted against a line demonstrating perfect return values (y = x) 39
Figure 4.5 – Values of quipazine released using constant voltage from three conditions of PPy (n=3 each) into PBS as measured using the HPLC-QQQ method..... 40
Figure 4.6 – Average concentrations of released quipazine from PPy films (108 mC deposition charge) triggered by cyclic voltammetry; equivalent data is depicted in two forms, by cumulative release (in blue) and by discrete release (in red) with appropriate standard deviations 41
Figure 4.7 – Concentrations of released quipazine from eight PPy films (108 mC deposition charge) triggered by cyclic voltammetry and color-coded by position on the MEA relative to the applied potential during film deposition (labeled '+' for the positive and '-' for the negative terminals)..... 42
Figure 4.8 – Concentrations of passively released quipazine from eight PPy films (56 mC deposition charge), coded by position on the MEA relative to the applied potential during film deposition..... 43
Figure 5.1 – Implantable device for local delivery of quipazine via PPy films..... 45

LIST OF TABLES

Table 1 – Reported optimal schemes for the electrodeposition of PPy 15

Table 2 – Reported optimal drug release conditions for PPy-doped films..... 16

Table 3 – Theoretical variability of exposed working electrode surface area 28

ACKNOWLEDGEMENTS

While attending the University of Washington, I have created an irreplaceable network of mentors, colleagues, and friends. First and foremost, I want to thank my primary advisor, Dr. Rajiv Saigal, who has been an invaluable source of clinical perspective, technical experience, and inspiration. I also thank Dr. Dale Whittington whose expertise and guidance was fundamental in utilizing mass spectrometry. Dr. Alberto Aliseda, my co-advisor, I thank for his consistent support in helping this research come to life.

My research team over the past two years has played a key role in cultivating this thesis. I want to thank undergraduates Max Walter, Alejandro Diaz, Jessica Johnson, Ben Healey, and Christine Hau. Additionally, graduate students Erin Graf and Joyce Huang, and visiting medical student, Richard Buksch, who helped collect data detailed in Chapter 4. Notably, I would like to thank the staff at the Washington Nanofabrication Facility, and the support provided by the Department of Neurological Surgery.

I give thanks to Dr. Sam Kassegne, Rita Youkhana, and their team at San Diego State University for collaborating on a prospective implant design, detailed in Chapter 5. I look forward to seeing what this partnership will bring.

Finally, nobody has been more supportive in the pursuit of this thesis than my family and friends. I thank my parents, Mike and Tammy Benoff, for their constant love and support that has made my academic career possible. Also, to the love of my life, Peter Link, who has been a steadfast source of joy, advice, and sometimes-fun facts.

Chapter 1. INTRODUCTION

1.1 PROJECT MOTIVATION

The actions and sensations of daily life are crafted by the spinal cord, a thin column of nervous tissue that sends and receives nerve signals [1]. After a spinal cord injury (SCI), commonly caused by fractured or dislocated vertebrae [2], signal transmission is disrupted; this may alter movement, feeling, and even involuntary functions critical to the body, depending on the location of the injury. In the United States alone, there are approximately 17,800 new cases of SCI annually [3], yet there is currently no clinical treatment available to improve functional movement. In recent years, functional electrical stimulation has shown promise in clinical trials as a rehabilitative technique [4-6]. Emerging experimental strategies have combined electrical stimulation with targeted drug delivery [7, 8], including quipazine, a drug that affects smooth muscle contraction [8-10]. Because of the combined chemical and electrical stimuli, this treatment may help uncover functionality previously inaccessible after injury, as demonstrated in rodent models of SCI [10]. Given the vast number of potential stimulation and drug delivery paradigms, there is a present need to further explore multimodal treatment strategies.

Conductive polymer thin films have been used in various biomedical applications for targeted drug delivery [11-14]. By undergoing oxidation-reduction reactions, conductive polymers can contain and release bioactive molecules [11, 15, 16]. In applications for the central nervous system (CNS), polypyrrole (PPy) has grown in popularity due to its biocompatibility [17, 18]. PPy has been doped with steroids to treat inflammation in the CNS of rodents after implantation of an electrode [16] and after SCI [19]. However, there has been no published research on the delivery of quipazine by PPy, or any other conductive polymers, in spite of its relevance to CNS injury.

1.1 Thesis Aims and Organization

The purpose of this thesis was to engineer a platform to study the delivery of quipazine by polypyrrole (PPy). This report begins with an introduction to SCI treatment, the role of microfabrication in drug delivery, analytical techniques for drug quantification, and conductive polymer mechanisms. It then highlights the design of a microfabricated, multielectrode array (MEA) to facilitate the deposition of conductive polymer thin films. This design was validated through examination of thin film morphology and drug delivery release. Because of the novel nature of this approach, we partnered with analytical chemistry experts to create a highly sensitive quantification method for quipazine. Preliminary experimental data is detailed near the end of this thesis. In the concluding chapter, an implant design is proposed to translate the PPy-quipazine thin films into *in vivo* experiments. Although the treatment of SCI motivated this thesis, the platform and methods hereafter can be translated to study any conductive polymer and prospective drug dopant.

Chapter 2. LITERATURE SURVEY ON MICROFABRICATION & TECHNIQUES IN DRUG DELIVERY

2.1 INTRODUCTION

Neuromodulation is the process of applying chemical and/or electrical stimulus to the central nervous system (CNS). Since neuromodulation can impact neuroplasticity, the brain's ability to adapt and form novel neural connections, there is great interest in its translation to treat SCI. This chapter provides an overview of devices and methods for electrical and chemical neuromodulation, the latter of which is achieved through drug delivery. Since both techniques often utilize micro-electro-mechanical systems (MEMS), several example devices and relevant microfabrication processes are highlighted. Additionally, the CNS-altering drug, quipazine, is introduced for its relevancy to later chapters. The core of this chapter focuses on the manufacturing and use of conductive polymer thin films, a unique family of materials capable of both forms of neuromodulation.

2.2 SPINAL CORD INJURY AND TREATMENT

Advances in medicine within recent decades have increased survival rates and life expectancies after SCI [2]; however, statistics do not shed light on the day-to-day experiences of these individuals. Depending on the location of injury along the spine, a SCI can cause paralysis, loss of sensation, and altered autonomic function, like bladder control, which is largely unconscious. In general, the closer the injury is to the head and neck, the more severe the outcomes are. Unfortunately, there is currently no cure for SCI, and there are few clinical interventions which can improve functional movement or autonomic functions. This is due to the complex and delicate

nature of the spinal cord, a mysterious component of the body whose mechanisms are still not entirely understood.

Clinical treatment of a SCI begins as immediately after injury as possible, with the overarching goal to best improve an individual's long-term quality of life. To understand the state of the injury, a surgical team will first visualize the spine and mechanically stabilize any damaged bone with specialized fasteners. After closure of the surgical site(s), the patient recovers in an intensive care unit (ICU) and receives pharmaceutical drugs as necessary to reach postoperative goals. These goals include relevant biological parameters, like mean arterial pressures, as determined by the care team [20]. Although no engineers are a part of this critical treatment process, it is important context to inform future device designs and interventions.

Existing chemical neuromodulation options are limited for the treatment of SCI. In fact, there is only one Food and Drug Administration (FDA)-approved pharmaceutical for SCI, the steroid Methylprednisolone. Due to debate over the treatment's efficacy, its use in recent years has declined, however [21]. Methylprednisolone has been associated with an increased risk to develop pneumonia and sepsis, a life-threatening infection [22]. To drastically reduce such systemic side effects, drugs used for the treatment of SCI may benefit from a more advanced delivery technique than traditional intravenous (IV) administration.

2.2.1 *Electrical Stimulation for Rehabilitation*

Functional electrical stimulation (FES) is a family of therapeutic techniques broadly used for pain management and rehabilitation. In recent years, epidural electrical stimulation (EES) has emerged as a prospective therapeutic modality for chronic treatment of SCI [4-6]. To deliver stimulation, an EES device was surgically implanted above the dura, the protective sheath surrounding the spinal cord. Currently, most research on EES utilizes an FDA-approved device by

Medtronic. In human clinical trials, EES combined with intense physical therapy aided functional recovery of movement; depending on the individual, this included independent standing and trunk stability [6], with some participants achieving over ground walking [4, 5]. Because of the promise FES could hold for improving movement and autonomic function, the advancement of stimulating devices is a highly active area of research for the treatment of SCI.

2.3 The Role of Microfabrication in Controlled Drug Delivery

Recently, there has been an explosion in research exploring chemical neuromodulation treatments for CNS injury [7, 15-17, 19, 23]. At the heart of this movement is localized drug delivery, the process of administering compounds directly to the tissue site of interest. By lowering the total amount of drug delivered to the body, a localized intervention can cause a therapeutic effect with a substantially lower risk of off-target effects than if delivered systemically. Platforms for controlling local drug delivery have been developed largely through techniques in microfabrication [24]. Microfabrication can produce systems with complex functionality and small feature sizes, often at or below the micron scale. These technical capabilities are necessary to precisely control small amounts of compounds and volumes. Ideal release systems also control for parameters including drug release patterns, like pulsatile vs. continuous release, since these can impact therapeutic response [25, 26]. However, there is a general lack of information illuminating the impact of drug release behavior on prospective treatments for SCI. The following sections highlight relevant manufacturing techniques and devices helping to contribute to this unknown space.

2.3.1 *Microfabricated Devices*

The growth of microfabricated, electrically controlled devices was largely impacted by the work of Professor Robert S. Langer, the most cited engineer in history [27]. An early device by Prof. Langer's team leveraged a micro-reservoir system with a dissolvable seal for controlled, small scale delivery of liquid drugs [28]. The system was comprised of pyramidal reservoirs etched out of a flat, silicone substrate. These reservoirs contained solutions under a thin, dissolvable gold membrane. When an applied potential was within the corrosion region of gold, the membrane dissolved. Although this mechanism allowed for pulsatile release, there was no method for modulating release profiles to precisely control delivery. Additionally, the device performance was highly sensitive to membrane material defects, rendering the method largely unadopted.

More recently, a team from Xiamen University developed a microchip with heightened spatiotemporal control of drug delivery [14]. The silicon substrate-based microchip had a 3 x 3 square array of electrodes with dimensions of 300 µm x 300 µm. These microelectrodes could be independently controlled for drug delivery through actuation of a conductive polymer. Polypyrrole, described in detail in section 2.6, was used to control two different model compounds through unique chemical properties. Total release was evaluated for each drug in response to a variety of parameters, including release pattern, via the comparison of cyclic voltammetry and potentiostatic conditions, and varying polymer layer thicknesses. These methods significantly motivated analyses contained within the primary content of this document.

2.3.2 *Techniques of Microfabrication*

Most microfabricated release devices are manufactured using the same basic processes, one of which includes photolithography. Photolithography is the process of transferring a pattern onto a substrate using a light-sensitive polymer, or photoresist. In some applications, a mask is

used to block light and selectively expose areas of a thin layer of photoresist. In direct-write lithography, a laser is directed to precisely expose photoresist regions and create complex designs [29]. In both techniques, the photosensitive polymer is first coated on the substrate surface, often using a rotating plate (Figure 2.1) and then baked in an oven. Note that in the below images, the environment is illuminated by a yellow light to prevent premature exposure to the photoresist. Depending on the type of applied photoresist, either the exposed or unexposed area on the substrate becomes soluble. In the case of positive photoresist, the direct-write tool exposes areas resembling the intended design. The unexposed polymer does not adhere to the substrate, so it may be removed when submerged in a solvent like acetone. This step is useful to build up features after processes like metal deposition, another critical step for production of electrically controlled devices.

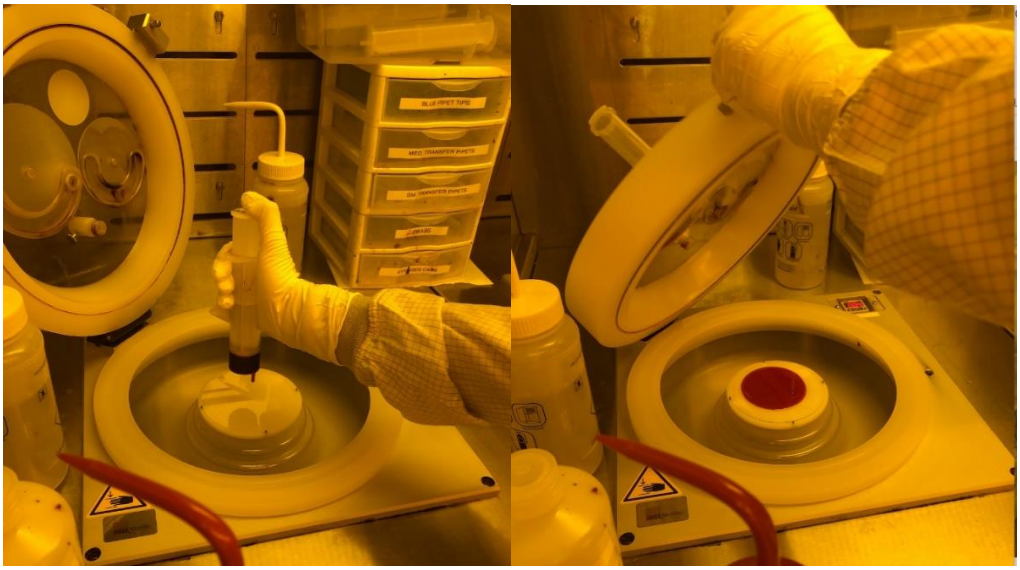

Figure 2.1 – (left) dispensing photoresist via a syringe onto a quartz substrate, (right) closing the lid of an automatic spin coater to evenly spread the photoresist

One technique in metal deposition directly relevant to our research is electron beam metal evaporation. In this process, an electron source within a vacuum-sealed chamber is focused on a crucible containing solid material, like titanium or gold. The crucible temperature is then increased to the material's point of evaporation or sublimation [30]. Substrates within the chamber will

receive a uniformly deposited layer of metal, with thicknesses on the order of tens of nanometers, as the material condenses (Figure 2.2). The coated substrate is then removed from the chamber and either etched away or lifted-off; in the latter, the substrate is submerged in developer to dissolve off any unbound photoresist, thus leaving a design of metal. Depending on the final device application, next steps after metal deposition may include specialty assembly techniques, like substrate cutting, or final processing, like cleaning within a solvent bath.

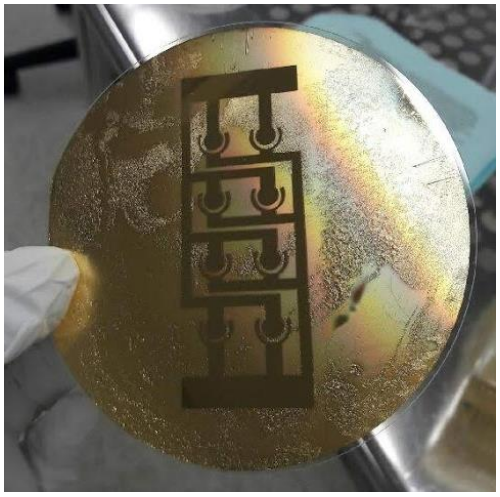

Figure 2.2 – Substrate held by a gloved researcher after the deposition of gold, highlighting the photopolymerized design visible at the center

2.3.3 *Advancing Electrode Materials*

Devices in the electrical and chemical neuromodulation space often utilize electrodes. To keep up with the increasing demand for high-quality, ever-shrinking devices, a new electrode manufacturing technique has emerged. A research team from San Diego State University has developed a method to transfer glassy carbon (GC) electrodes onto a flexible, biocompatible polymer [31]. Previously, use of GC was restricted to applications on stiff substrates inappropriate for implantation. However, the superior *in vitro* performance of GC in comparison to traditional platinum makes it a prospective material for neural stimulation applications [32]. Highly relevant

to this thesis was the inclusion of the conductive polymer, PEDOT, as a top layer over the GC electrodes. A technique common for microelectronics, the conductive polymer helped maintain impedance levels after miniaturization of the electrodes. Because conductive polymers can also be used for drug transport, this manufacturing method could be leveraged to develop a biocompatible, implantable stimulator with the capacity for targeted drug delivery.

2.4 Delivery of The Experimental Drug, Quipazine

Quipazine, an experimental drug that activates serotonin receptors, has been studied in animal models since the late 1960's for its influence on the CNS [33]. When administered, quipazine binds to serotonin receptors to produce a biological response, thus increasing cellular excitability. This heightened excitability motivated its initial use as a treatment for SCI. During the 1990's, quipazine was shown to improve treadmill locomotion on spinal cord-transected cats [34]. In several studies exploring the impact of quipazine and training after complete spinal injury, quipazine was administered intraperitoneally, or through the abdomen, to complement robotic movement training of mice [9, 10], and to aid functional electrical stimulation of rodents [8, 10].

2.4.1 *A Multimodal Device for Chronic SCI*

A big advancement in research for the treatment of SCI was a first-of-its-kind multimodal implant named the "e-dura" [7, 10]. The e-dura was designed for implantation below a rodent's dura after experiencing a SCI. The body of the e-dura was a flexible, flat silicone substrate containing platinum-silicone electrodes (300 µm in diameter) with gold interconnects and a compliant tube for drug delivery [7]. The tube mediated targeted quipazine administration via an external injection. Although highly controversial if proposed for human use, this approach facilitated an unprecedented study of both chemical and electrical neuromodulation.

In a rodent model of chronic, or long-term, SCI, the e-dura was used to compare the effects of training, serotonergic modification (via quipazine), and electrical stimulation on function, behavior, and histology [10]. As shown by histology, the study of tissue structures, the trained rodents had a reorganization in neural circuitry near the injury site; however, this adaptation did not facilitate functional movement. In comparison, when injected with quipazine and electrically stimulated, rodents regained coordinated movement in multiple trained tasks. Thus, the key to exciting functionality in the injured spinal cord was the combined electrical and chemical neuromodulation [10]. Current research to advance the treatment of SCI is parsing out the effects of combining electrical stimulation, drug delivery paradigms, and rehabilitation protocols on recovery of functional movement.

2.4.2 *The Barriers of Quipazine*

Since quipazine is still an experimental drug, its use must be extensively characterized in animal models. Prior work has not agreed upon a therapeutic dosage for rats after SCI, with observations of 0.3 mg/kg [8] and 0.5 mg/kg [9] to both achieve ideal responses with functional stepping. For spinal cord transected mice, the ideal dosage was observed to be a bit higher, at 1 to 2 mg/kg [35]. Furthermore, there is not substantial evidence on the selection of localized versus systemic quipazine delivery, although the most extensive study utilized targeted delivery [7]. An underlying requirement in these studies is a live participant or sample; consequently, there is a lack of information on how to directly measure quipazine. The chemical structure of serotonin can be measured and used as an indicator for quipazine effects using high-performance liquid chromatography coupled to electrochemical detection (ED), a highly sensitive system based on chemical reactions [36] (see section 2.5.2); however, there is a need for the direct measurement of

quipazine for more rapid experimentation without the reliance on expensive, time-intensive means like animal husbandry.

2.5 Quantifying Drug Delivery

In the field of drug delivery, quantification techniques vary greatly in specificity, the ability to correctly identify negative results. Choosing an appropriate analysis technique is of the utmost importance, particularly when validating localized delivery systems with small absolute values of released drugs [15]. For microfluidic techniques, this can be relatively straight forward since flow rates can be computed to calculate dosages under ideal conditions. However, for many systems, computation of released dosages is often not practical or accurate. Applications interested in biological responses can use cell behavior and byproducts as an indicator for drug presence, but this is an indirect method not possible for all compounds of interest. The following sections overview two relevant quantification techniques for drug delivery.

2.5.1 *Ultraviolet-visible Absorption (UV-vis) Spectroscopy*

UV-vis spectroscopy measures the absorbance of light in a solution or gas to determine analyte concentration [37]. Using Beer's law under controlled experimental conditions, absorbance is proportional to concentration. Thus, a linear reference can be used to determine concentrations of unknown samples based upon measured absorbance values. This technique can be very useful when compound(s) dissolved in solution have unique wavelengths for peak absorbance. However, the measurement of absorbance does not discriminate between drugs of interest and other molecules in solution with overlapping absorbance spectra [38]. This lack of specificity can produce overestimated results when used as a standalone technique.

2.5.2 *Mass Spectrometry*

High-performance liquid chromatography (HPLC) coupled with mass spectrometry (MS) is an analytical chemistry technique that combines mass analysis and physical liquid separation to sort and measure components in a solution. In HPLC-MS, a volume of sample is first introduced into the system, usually by an autosampler. This sample is delivered to an HPLC column using various solvents. The sample and solvent mixture is then pumped through a column under high pressure, causing interactions with the column depending on various physical and chemical attributes. In reverse-phase HPLC, the most universally used method, polar compounds elute, or are removed, off the column much more rapidly than non-polar compounds. After eluting, the sample is introduced into the mass spectrometer using electrospray ionization, a process that creates charged droplets. As the droplets evaporate, a charge is induced on the molecule. These charge ions are then manipulated through the mass spectrometer using electric fields to provide a mass-to-charge (*m/z*) ratio for the parent ion. Depending on the type of analyzer on the mass spectrometer, the parent ion can be used to determine chemical formulas to aid compound identification. A variety of mass spectrometers are also embedded with collision cells, technology that fragments selected parent ions to produce daughter ions. A triple quadrupole (QQQ) mass spectrometer incorporates a collision cell to increase the identifiable mass range and scan rate of samples available.

A chromatogram depicts relevant MS data used to quantify analytes of interest (Figure 2.3). Along the horizontal axis of a chromatogram is retention time, provided in minutes; this is a measure of how long an analyte took to pass through a chromatographic column. Retention time should be consistent with every sample injection for HPLC. Intensity determines the magnitude or “peak” of a chromatogram, as it is a measure of the presence of a specific ion, either parent or

daughter. The integral of a single peak is linearly proportionate to the compound's concentration in solution. Samples with known concentrations of analyte can be used as a reference to determine unknown concentrations.

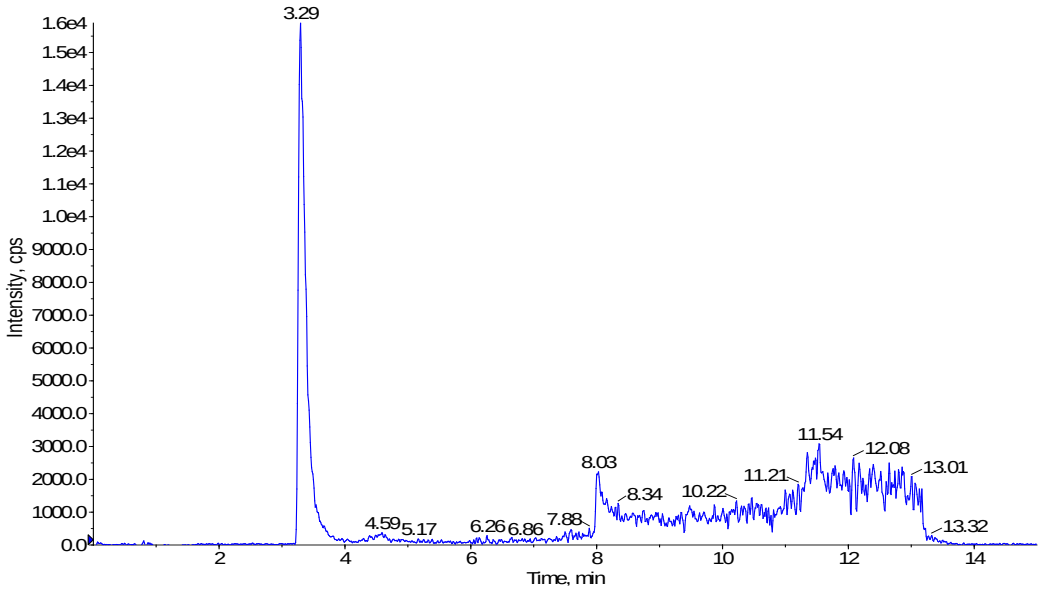

Figure 2.3 – Example total ion chromatogram produced using methods found in Chapter 4

HPLC-MS allowed for the recent identification of components released from two conductive polymers, PEDOT and polypyrrole [38]. Contrary to previous belief, conductive polymer films release more than just drugs of interest; at least three categories of compounds were released from both polymers. The first grouping to elute off the column were ions from the buffer solution, followed by the expected drug, and then, finally, unexpected free monomers. Unlike UV -vis spectroscopy, HPLC-MS has very low limits of detection (LOD) and quantification (LOQ), the concentration limits that the system can identify a compound and quantify its amount, respectively.

2.6 Conductive Polymers

Polymeric systems using mechanisms like diffusion, chemical degradation, and external activation have been widely utilized for applications in drug delivery [25]. Of the systems that are

externally activated, conductive polymer (CP) films have been widely studied for controlled drug delivery due to their unique redox properties and relevancy for implantable devices [11, 12, 14, 17, 39]. Through application of an external potential, CP films can be switched between oxidized and reduced states, thus facilitating the transport of bioactive molecules [11, 15, 16].

CP films are manufactured using an electropolymerization process. Positive current is first applied through an aqueous solution containing monomers and anionic dopant(s) of interest (Figure 2.4). If a drug of interest is not anionic, a packaging method, like the inclusion of the molecule, biotin, can be used to adjust the compound to an appropriate charge [12]. During oxidation, dopants incorporate into the positively charged polymer backbone to create a film. When a sufficiently large negative current is applied, the polymer is reduced and the anionic dopants are repelled into the environment [11, 15]. During state cycling, CP films will also expand or contract in volume due to the movement of hydrated ions [16].

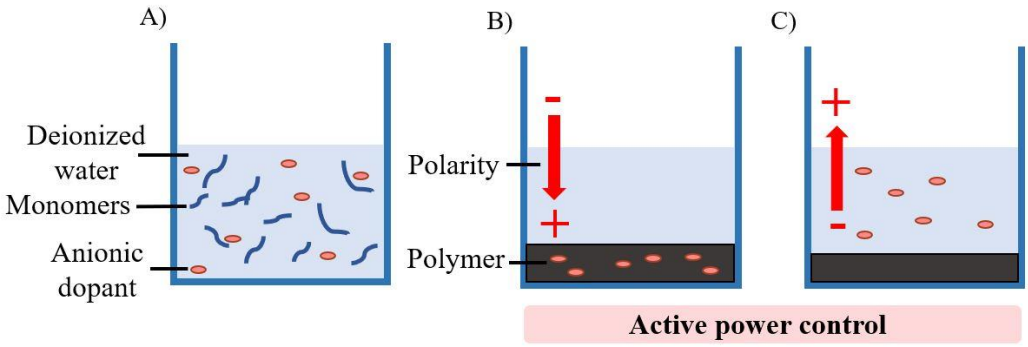

Figure 2.4 – Schematic of conductive polymer states, (a) passive electrolyte solution (b) oxidized film and (c) reduced film with released dopants

2.6.1 *Polypyrrole*

Polypyrrole (PPy) is a conductive polymer popular in biomedical applications because of its easy electrosynthesis from solution, good stability, and biocompatibility [11, 16]. Like all conductive polymers, the ionic transport capability of PPy is heavily dependent on its

electrosynthesis conditions [11]. By adjusting electrical parameters and including compounds, it is possible to *tune* doped PPy. However, this process is highly specific to any given compound's chemistry, so electrodeposition parameters must be optimized for every unique solution.

Several studies have characterized the release of compounds from polypyrrole, as highlighted in

Table 1. Within the detailed publications, the most common method for depositing PPy utilized potentiostatic, or constant potential, conditions on an aqueous solution of either 0.1 M or 0.2 M monomer. There is less of a consensus on applied potential settings, however. Theoretically, polymerization charge, the ratio of electric charge delivered per unit area, is proportionate to cumulative drug release; this was demonstrated experimentally with the steroid, dexamethasone phosphate, and the conductive polymer, PEDOT [26]. Therefore, polymerization settings are often a variable of interest when studying new dopants or trying to understand drug release performance.

Table 1 – Reported optimal schemes for the electrodeposition of PPy

Pyrrole Concentration	**Dopant(s)**	**Reference**	**Applied Potential**	**Setting**
54 mM	0.5 M sulfuric acid (H_2SO_4)	[40]	Potentiostatically	4 mA/cm^2
0.1 M	0.1 M sodium tosylate (NaTOS)	[11]	Potentiostatically	2 mA/cm^2
0.1 M	0.1 M dexamethasone disodium phosphate	[17]	Potentiostatically	25–30 mC/cm^2
0.1 M	0.025 M dexamethasone disodium phosphate	[16]	Potentiostatically	700 mC/ cm^2
0.1 M	6.82 mM penicillin/streptomycin	[41]	Cyclic Voltammetry	0 to +1.1 V at 100 mV/s
0.2 M	0.2 M sulfosalicylic acid (SSA)	[14]	Potentiostatically	2 C/cm^2
0.2 M	0.1 M p-toluene sulfonate (pTS)	[42]	Potentiostatically	180 mC/ cm^2

Experimental drug release conditions play an equally important role in determining the performance of drug doped PPy. Most notably is the application of voltage. Cyclic voltammetry (CV) has been shown to release significantly more drug in some instances when compared to direct-current, or potentiostatically-controlled, release [26]. Furthermore, CV scan rate impacts release behavior; lower scan rates released higher amounts of drug per cycle, whereas higher scan rates depleted the dopant more rapidly [17]. As highlighted in table 2, CV has been more common in recent publications for controlled release using PPy.

Table 2 – Reported optimal drug release conditions for PPy-doped films

Pyrrole Concentration	Dopant(s)	Reference	Applied Potential	Setting
0.1 M	0.1 M dexamethasone disodium phosphate	[17]	Cyclic Voltammetry	-0.8 V to +1.4 V at 100 mV/s
0.1 M	0.025 M dexamethasone disodium phosphate	[16]	Cyclic Voltammetry	-0.9 V to +0.8 V at 100 mV/s
0.1 M	6.82 mM penicillin/streptomycin OR 0.125 dexamethasone	[41]	Cyclic Voltammetry	-1 to +1 V at 100 mV/s
0.2 M	0.2 M sulfosalicylic acid (SSA)	[14]	Potentiostatically	-0.8 V
0.2 M	0.1 M p-toluene sulfonate (pTS)	[42]	Cyclic Voltammetry	±0.6 V at 0.5 Hz

The inconsistency of reported values between studies on PPy for drug delivery makes objective comparisons difficult. By observation across conductive polymer research, local drug delivery results seem to be most often reported as concentrations. Of the references listed within table 2, two studies reported maximal drug release concentrations on the order of 16 μg/cm^2 [17] and 100 μg/cm^2 [16]. In comparison, the remaining referenced studies used either theoretical loading percentages [14, 41] or release rate [42]. The diversity in result depictions poses a challenge for researchers establishing methods for new PPy film dopants. Consequently, the drug

release targets established with this document have been selected methodically, based upon limited published references.

2.6.2 *A Chamber Device to Manufacture and Test PPy*

Although drug release using conductive polymers has been explored *in vitro* and *in vivo* for a variety of compounds, there are still a lot of unknowns preventing the use of PPy in devices for the CNS [26]. To tackle one unknown, the effect of electrical stimulation paradigms on cells, a team from Massachusetts Institute for Technology (MIT) created a PPy cell-culture chamber [43]. This chamber, designed for *in vitro* high throughput testing, consisted of a polydimethylsiloxane (PDMS) insert with eight cylindrical holes sealed to an indium tin-oxide (ITO) conductive slide (Figure 2.5). To manufacture PPy, the ITO slide was completely submerged in a separate monomer solution of pyrrole. The PDMS and ITO slide were then clamped together using two polycarbonate plates to create eight unexposed columns or wells. When connected to a power source, various stimulation parameters could be run beneath cells seeded in each well.

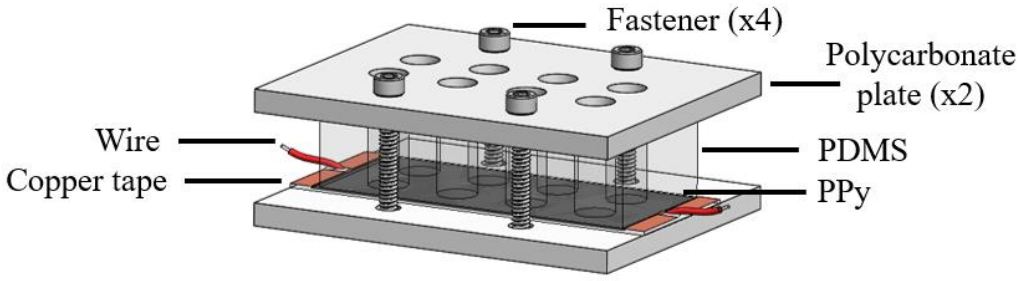

Figure 2.5 – The polypyrrole cell chamber with an ITO slide covered in dark polypyrrole

Since the cell chamber was developed during Dr. Rajiv Saigal's graduate research, this device was also used in preliminary work for the main component of this thesis. The described cell chamber was a useful learning tool to practice the manufacturing process of polypyrrole. The simplicity of the design was very user friendly and facilitated preliminary experimentation with model drugs. However, after examining drug release samples using UV-vis spectroscopy, the

repeatability of drug release values was poor. Upon further exploration, the PPy film thicknesses were uneven across the ITO slide, presumably allowing different dopant presence depending on well position. In short, each doped sample could vary under the same electrodeposition scheme. These issues motivated the addition of a microfabricated component to improve spatiotemporal control over PPy manufacturing. By incorporating a new component to deposit films on, we could take advantage of the simple, biocompatible chamber concept.

Chapter 3. A MICROFABRICATED PLATFORM FOR CONTROLLED DRUG RELEASE FROM POLYPYRROLE

3.1 CHAPTER OVERVIEW

To manufacture then test conductive polymer films under novel experimental conditions, we developed a microfabricated platform. This platform utilized a custom multielectrode array (MEA) to produce up to eight films. The design requirements and manufacturing process for the MEA is included within this chapter. This chapter also provides preliminary information on the quality of PPy films, including topographical and morphological results. Although we created polypyrrole doped with the model drug, quipazine, this platform can be implemented to study numerous other variations of drug-doped conductive polymers.

3.2 THE DESIGN AND MANUFACTURING OF A MULTIELECTRODE ARRAY

The first aim of this thesis was to design a platform for manufacturing and testing PPy films doped with the model drug, quipazine. Design requirements for this platform were (i) to use materials that could be sterilized for future testing with cells, (ii) to manufacture multiple PPy films uniformly from solution, and (iii) to require a single power source. Although disposable electrodes are available commercially, we were not satisfied with the products we sampled; these products either could not withstand our experimental protocol, produced irregular films, or were cumbersome to adapt for depositing PPy. For example, after undergoing our protocol, an 8-electrode gold array (Applied BioPhysics, NY, USA) delaminated from its underlying polycarbonate substrate.

3.2.1 *A novel design*

As is common for the study of conductive polymer films [24], we utilized techniques in microfabrication to create a MEA. This design was inspired by several existing devices, including commercially available gold arrays, disposable gold electrodes [44], and the PPy cell chamber described in section 2.6.2. Design constraints were centered around self-sustainability, such that all MEAs were to be manufactured on site at the Washington Nanofabrication Facility (WNF). This established the restrictions that all MEAs needed to fit on a standard-sized circular substrate with diameter of 100 mm and would not require any outsourcing beyond the purchasing of materials. Additionally, we chose to develop a MEA compatible for use with components of the PPy cell chamber. Thus, each repeating electrode element of the MEA needed to fit within a circle of diameter 7.7 mm exposed by the PDMS insert.

The MEA, designed using Layout Editor software (Unterhaching, Germany), had outer dimensions of 74.40 mm x 13.75 mm and contained eight repeating elements (Figure 3.1). Each electrode cell was composed of a circular working electrode and a crescent-shaped counter electrode. 3 mm wide inner tracks connected all eight of the working or counter electrodes in parallel. When pyrrole monomer solution connected the two electrode elements, the powered MEA would deposit PPy films on the working electrode surface. Then, when the polarity was switched such that the working electrode was negatively charged and the counter electrode was positively charged, the films would repel their anionic dopants. The MEA design eliminated lead times associated with commercial products and provided full control over electrode surface roughness and sterility.

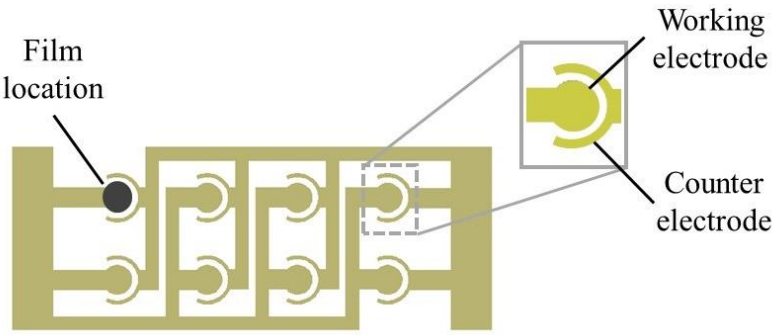

Figure 3.1 - The microfabricated electrode array design with 8 parallel electrode cells and a simulated PPy film for reference

3.2.2 *Microfabrication*

We manufactured MEAs in nine steps using microfabrication processes at the WNF as highlighted in Figure 3.2. Manufacturing began with surface preparation of a 100 mm silica (quartz) substrate (University Wafer, MA, USA) baked in hexamethyldisilazane (HMDS). We then applied positive photoresist (Microchemicals GmbH, Ulm, Germany) and used an automatic spin coater (Suss Microtec, Garching, Germany) to create a uniform layer. Immediately following, the photoresist was baked at 100 ºC for 180 sec in an electro-polished hot plate. To produce the characteristic MEA design, we polymerized the photoresist with a direct write laser (Heidelberg Instruments, Heidelberg, Germany). We then quickly immersed the substrate in developer solution and subsequently rinsed it through a cascade bath of water. The substrate was then spun dry in an automatic drier. At this point, substrates could be stored for up to several weeks without impacting their integrity.

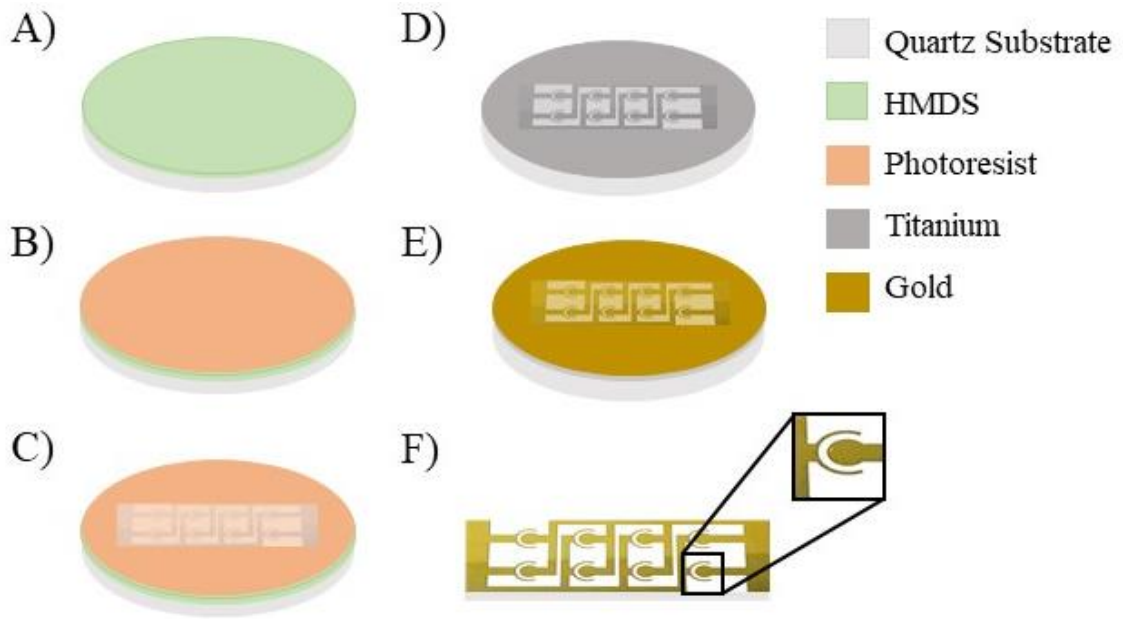

Figure 3.2 – A schematic of the main MEA microfabrication processes, (a) preparing the wafer surface with HMDS (b) applying photoresist (c) exposing a single array design (d) depositing titanium (e) depositing gold (f) dicing of the final array with feature inset of a single electrode

After lithography, we performed the final key processes to bring the MEA to life. This began by placing the developed substrate into an electron-beam metal evaporation system (CHA Industries, CA, USA) to deposit an adhesion layer of titanium (50 nm) and a bulk layer of gold (250 nm). The substrate was then submerged in an acetone bath for a minimum of 12 hours to lift off metal lying beyond the polymerized array design. After the removal of all undesired metal, we air-dried the substrate and spun a uniform protective layer of photoresist on the design side. We then applied a single layer of tape to the underside of the substrate. The wafer was cut to size by a semiautomatic dicer (Disco America, CA, USA) equipped with a diamond blade. The final MEAs were immersed in an acetone bath for several hours and then checked visually for any imperfections prior to experimental use. Overall, each substrate required approximately three days of processing.

3.2.3 *Lessons learned in manufacturing*

To develop a robust manufacturing protocol, we combined fundamental principles in microfabrication with experimental observations. During initial MEA prototyping, we focused on improving material selections. For example, we began MEA manufacturing on silicon substrate, as this is a common choice for microelectronics. However, silicon was too conductive for experimental use (see section 3.3.1), so we were not successful in depositing films on the working electrode. After switching to quartz substrates, we were able to control the flow of current and create PPy films as intended. Once we had this successful design, we produced two MEAs per substrate to improve throughput with negligible impact on net cost.

As we ramped up MEA production, we faced challenges in MEA reproducibility. The first of these issues was observed while manufacturing; if left in storage for too long after applying photoresist, the substrate's coating changed in consistency. This inspired the restriction on allowable down time between processes, a conservative limit of 2 days for substrates with photoresist stored in a light-blocking container. We also eliminated down time for undeveloped designs, produced by the direct-write laser, as this increased the risk of uncontrolled exposure to light. A second, more obscure issue was brought to light during experimentation with the MEA. Initial prototypes with 150 nm of deposited gold would produce films inconsistently. Upon further analysis, we noted that resistance measurements varied across the MEA; by increasing the gold deposition thickness to 250 nm, we ensured appropriate film deposition for all eight working electrodes. These highlighted changes decreased variability and improved experimental performance, overall.

3.3 Electrochemical Manufacturing of PPy Films

To accommodate the unique deposition process for conductive polymers, we constructed experimental chambers (Figure 3.3). The workhorse of each chamber, our MEA, provided the key connection to a DC power supply (Keysight Technologies, CA, USA) to facilitate film deposition. To prepare the MEA for experimental use, we first cleaned the surface with isopropanol alcohol (IPA). After air drying, we attached strips of copper tape and soldered wire to the shortest ends of the MEA. This established contact sites to the power source. The MEA was then placed on top of a flat polycarbonate plate for alignment with the PDMS insert.

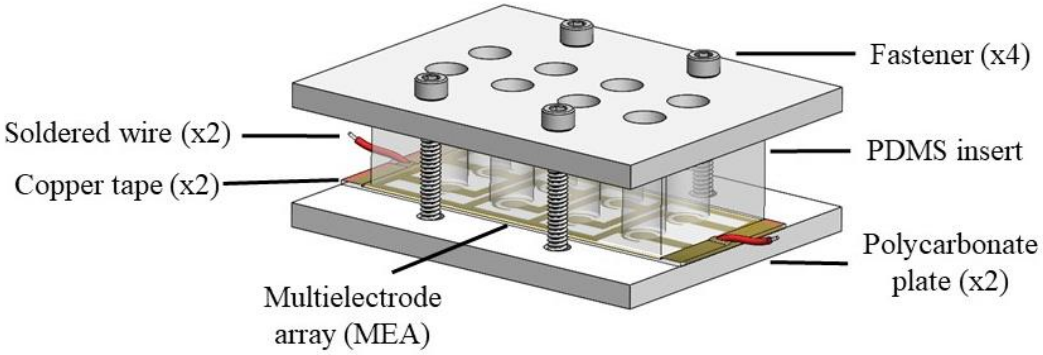

Figure 3.3 – Experimental chamber with two polycarbonate plates, a PDMS insert, and a MEA creating 8 independent wells

The PDMS insert contained pyrrole monomer solution above each electrode pair to facilitate film deposition and later drug release experimentation. PDMS was selected for its ease of manufacturing, ability for sterilization, and gasket-like behavior under pressure. We made inserts approximately one day before assembling an experimental chamber, by combining a 10:1 ratio of elastomer base and curing agent (Dow Sylgard 184), then pouring the viscous mixture over a custom mold (Figure 3.4). The base of the mold was an aluminum rectangle (73 mm x 40 mm top surface) with eight threaded holes to house shoulder screws (5/16” diameter, 2” shoulder length5/15”-18 thread). The mold was wrapped in tin foil then baked at 80º C for 2 hours. After

baking, the insert was carefully removed for later experimental use. Although PDMS is a popular material for microfluidic devices and various other biomedical applications, there is some evidence that it can alter drug concentrations; this is because hydrophobic chemicals may bind to exposed surfaces [45]. Should this phenomenon pose a challenge in the future, we would implement surface preparation steps with each insert prior to all experimentation.

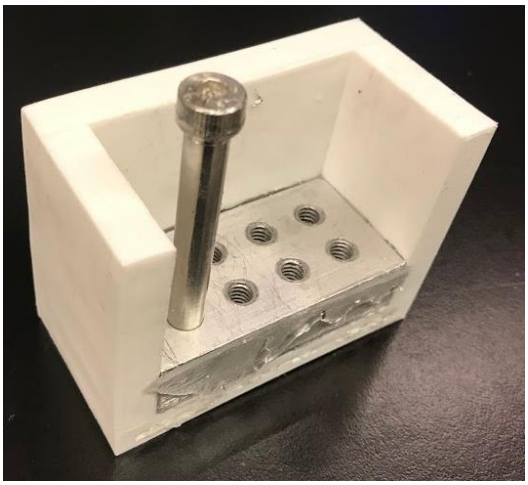

Figure 3.4 – The PDMS curing mold, with 3D printed side walls, an aluminum base, threaded sites for 8 fasteners, and one shoulder screw in place for example

After preparing the PDMS insert and MEA, the experimental chamber was assembled for use. To ensure all components were thoroughly cleaned, we first soaked the polycarbonate plates and PDMS insert in a precision-cleaning detergent (Alconox, NY, USA) for a minimum of 30 minutes. These items were then rinsed thoroughly with IPA and air dried. Next, each electrode pair of the MEA was carefully aligned to a well of the insert by visual inspection through the transparent bottom plate. The chamber was then fastened together using four nylon socket head screws (8-32 thread size, 1-3/8" long). During this step, we would secure the nuts of adjacent fasteners in an “x” fashion to prevent cracking of the MEA. The chamber was then visually inspected for leaks using deionized water. Immediately prior to experimental use, the chamber was

connected to the power source such that the working electrodes were positively charged, and the counter electrodes negatively charged, respectively.

3.3.1 *Experimental protocol for film deposition*

PPy films were created through electrosynthesis, the process of synthesizing chemical compounds using an electrochemical cell. Via our experimental chamber and MEA, we created eight individual cells in parallel. Each cell was comprised of a working electrode, a counter electrode, and monomer solution captured within a single well of the PDMS insert. Our stock monomer solution, hereafter denoted as pyrrole, was composed of 0.2 M Pyrrole (Sigma-Aldrich), deionized water, and 0.2 M Sodium Dodecylbenzenesulfonate (NaDBS) (Sigma-Aldrich) a surfactant added to lower surface tension. The inclusion of NaDBS allowed for greater amounts of quipazine to dissolve into the pyrrole solution.

The process for film deposition occurred in two steps. The first layer, also known as the adhesion layer, provided a drug-free surface to help the film bind to the working electrode. To create this adhesion layer, we pipetted 400 µL of pyrrole stock solution into a single well. We then delivered 1 mA of current for 30 seconds, producing a deposition charge of 30 mC. After deposition, we pipetted out all remaining solution then added 400 µL of pyrrole stock containing 10 mg/mL of quipazine (MiliporeSigma, Darmstadt, Germany) (Figure 3.5). To produce the bulk, drug-containing layer, we delivered 2 mA of current for either 28 or 54 seconds; this produced deposition charges of 56 and 108 mC, respectively. Throughout the remainder of this document, films were classified by the deposition charge used to create the bulk quipazine layer.

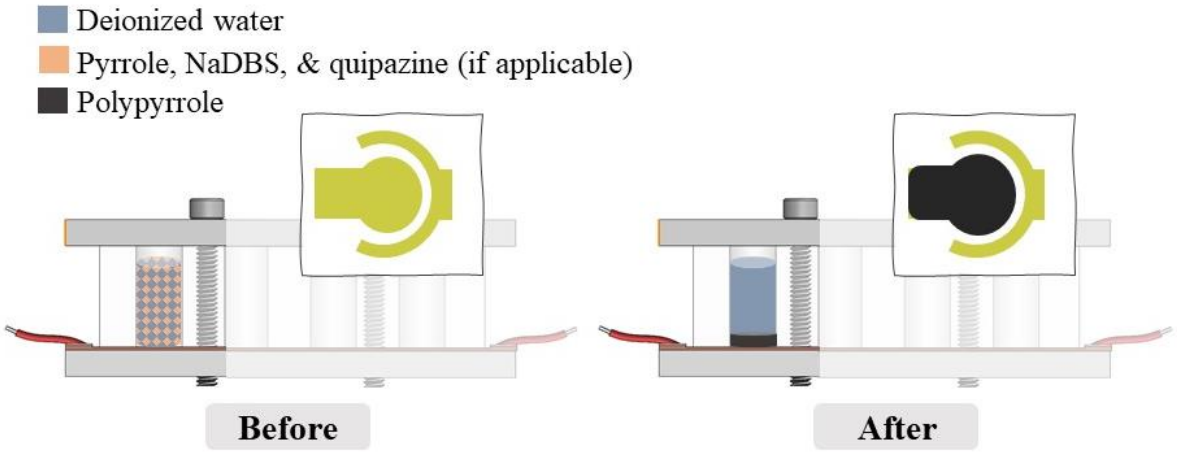

Figure 3.5 – Side view of the experimental chamber prior to electrodeposition (left) and after film deposition (right)

3.3.2 *Theoretical film size*

Film size was determined by the exposed surface of the working electrode during deposition. Consequently, there was some inherent variability in film sizes. As predicted using computer aided design software, possible working electrode surface areas were 21.41 ± 1.18 mm^2, depending on alignment of the PDMS insert. Thus, if the insert was aligned to allow for maximal and minimal exposure, there could be up to an 11% difference in exposed working electrode areas on a single MEA. The consequence of this variability is a range of polymerization charges, which correspond to film thickness (Table 3). To combat this potential for variability, each electrode pair on a MEA was cautiously aligned to the PDMS insert and verified visually prior to experimental use. Consequently, film sizes were likely much lower than 11%, a threshold we deemed acceptable for this application. Should future work require tighter tolerancing of the exposed electrode area, we would add an insulating layer of SU-8, a commonly used biocompatible polymer [46], on top of the MEA. All other methods would not be altered.

Table 3 – Theoretical variability of exposed working electrode surface area

Duration of 2 mA current (sec)	**Electric (deposition) Charge (mC)**	**Minimum Polymerization Charge (mC/cm^2)**	**Maximum Polymerization Charge (mC/cm^2)**	**Percent Difference (%)**
28	56	248.	277.	11.0
54	108	478.	534.	11.0

3.3.3 *Film Topography*

PPy films were deposited on two separate MEAs using deposition charges of 56 and 108 mC. Topographical information was then obtained using a DektakXT Profilometer (Bruker, MA, USA). We mapped films in 3D space at a constant speed of 1377 µm/s and a constant force of 1 mg (Figure 3.6). All data was postprocessed using the open-source software, Gwyddion (version 2.55) to extract film thicknesses. Measurements were zeroed to a 3-point plane generated from the quartz substrate. This substrate was removed from analyses using an inverted height threshold to generate a masked, excluded region. A convolution filter was applied to smooth the topographical data. To preserve the natural appearance of the film samples, we did not clean off any dust or debris remaining after deposition. Films were excluded from analyses if damaged during transportation or if debris present was large enough to be dragged by the stylus, thus potentially damaging the film surface.

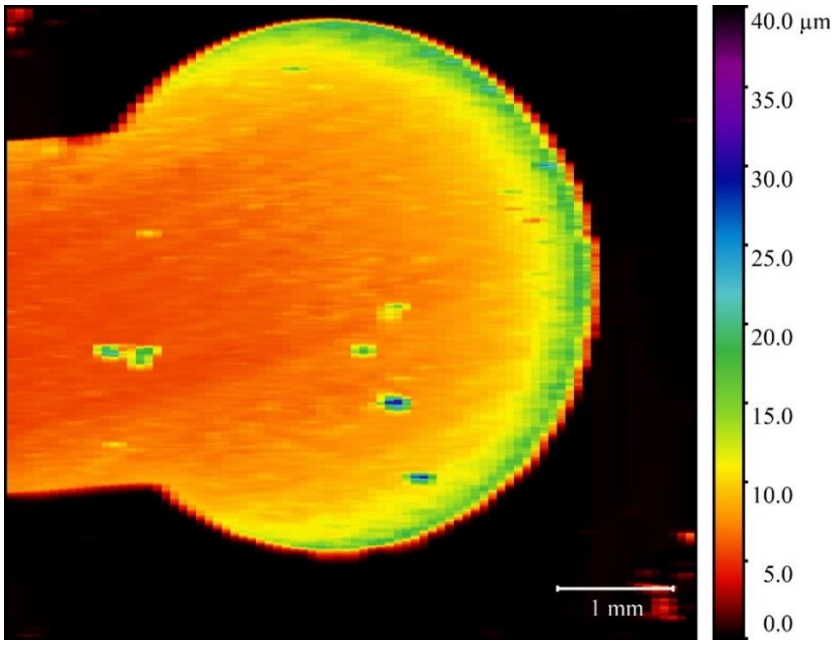

Figure 3.6 – Topographical image of a film deposited at 108 mC after undergoing cyclic voltammetry experimental conditions (scale bar is 1 mm)

Since polymerization charge determines film thickness [26], profilometry data gave insight into film variability. At the deposition charge of 56 mC (n=5), a single MEA produced films with an average height of 4.95 µm and standard deviation of 0.29 µm (Figure 3.7). In comparison, the deposition charge of 108 mC (n=7) produced an average film height of 8.20 µm and standard deviation 0.12 µm. Up to a threshold value, deposition charge should be proportional to average film height. Although the films produced at each deposition charge underwent two different experimental conditions, cyclic voltammetry for the 108 mC group and passive release in PBS for the 56 mC group, results were linear (Figure 3.7). Further exploration of film thicknesses is required to rule out any implications from experimental drug release conditions.

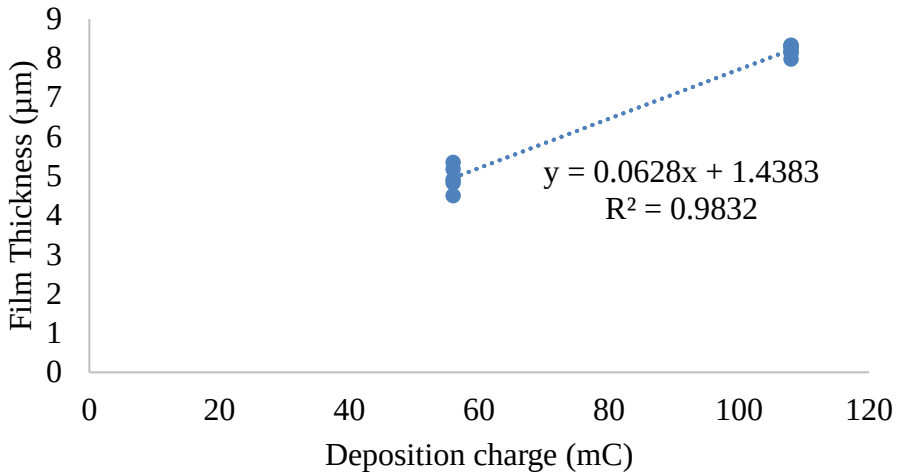

Figure 3.7 – Average thicknesses of thin films by deposition charge after experimental release conditions

3.3.4 *Film Morphology*

An important step in validating the MEA-based platform was to assess how film morphology compared to previous publications. Using a field-emission scanning electron microscope (SEM, Sirion XL30), we captured images of a film deposited at 108 mC (Figure 3.8). After undergoing cyclic voltammetry experimental conditions, a single film was removed from the MEA and taped to an SEM platform. The most prominent feature of this film sample was its hierarchical structure, indicative of applied potentials above 1V (Figure 3.8) [47]. This hierarchy, with previously described "microislands" and neighboring indentations, is a product of polypyrrole's redox reaction. In comparison to the microislands found over the bulk of the film, the film's perimeter was raised and possessed a denser structure (Figure 3.9). As seen from profilometry data, all films possessed this raised edge, but the different structure proved interesting. On the inner side of the edge, there was a densely packed, almost cracked-like appearance. At the outermost region of the film, the hierarchical structure returns, but on a smaller

scale. This heterogeneity may be dependent on the strength of the electric field during deposition since these edge effects are only located on areas closest to the counter electrode.

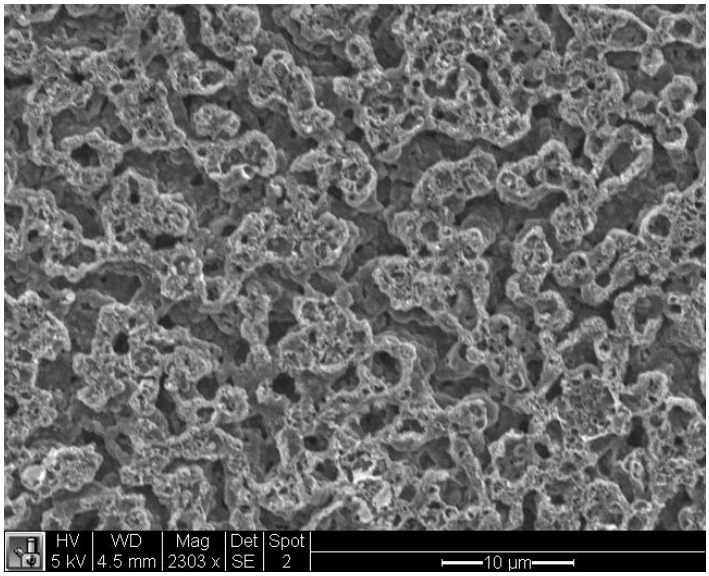

Figure 3.8 – SEM image of the center of a PPy film (deposition charge 108 mC) after undergoing cyclic voltammetry experimental conditions (scale bar is 10 µm)

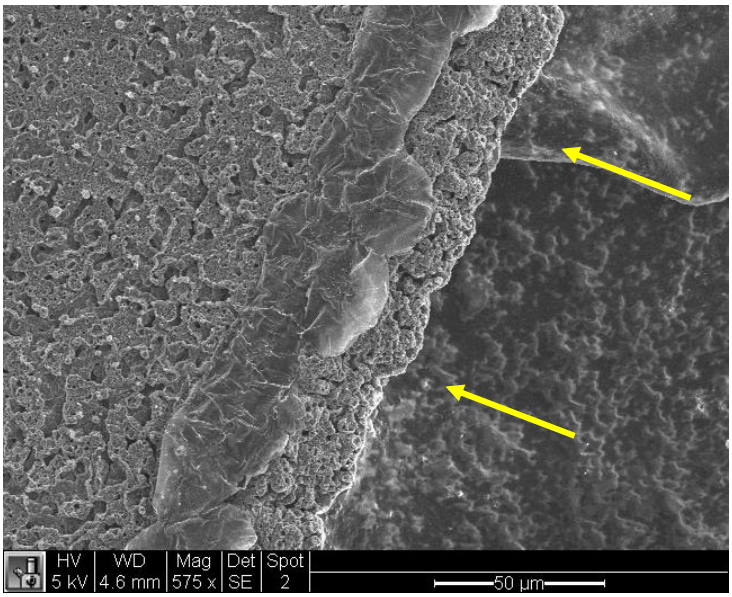

Figure 3.9 – SEM image a PPy film (deposition charge 108 mC) with arrows highlighting the outermost edge of the film (scale bar is 50 µm)

3.4 Discussion and Reflection

The novel platform we have developed to study conductive polymers was successful in two very different ways. The first success was pragmatic, to facilitate experimentation of new drug delivery techniques for the eventual use in animal models of SCI. The second, less explicitly stated feat, was to teach students fundamental manufacturing principles. In traditional mechanical engineering curriculum, manufacturing is visceral, with a focus on cutting, milling, and sanding metal alloys or wood. In comparison, nano- and microfabrication requires students to understand and operate complex machinery whose processes cannot always be seen with the naked eye. I believe that manufacturing at the micro scale has taught me a greater appreciation for appropriate material selection, scaling up production, and overall attention to detail.

Chapter 4. QUANTIFYING THE CONTROLLED RELEASE OF QUIPAZINE FROM PPY

4.1 INTRODUCTION

To test the performance of the MEA and associated PPy films, we explored quantification techniques and experimental protocols appropriate for use with quipazine. As described in section 2.4, prior research using quipazine has relied on living models to demonstrate behavioral changes or produce chemicals like serotonin. However, we desired a method that did not require the maintenance of living models. As detailed in this chapter, we simultaneously ran controlled release experiments and implemented quantification methods; this helped to develop robust protocols based upon actual samples of released drug. We initially released quipazine from PPy using constant voltage conditions then analyzed these samples using ultraviolet (UV) spectroscopy. After determining this technique inappropriate for our approach, we developed a HPLC- mass spectrometry method for validation of the MEA. Results from both measurement techniques are included within this chapter.

4.1.1 *Controlled release protocol*

The goal of each controlled release experiment was to repel anionic dopants from the PPy films. This was achieved by creating a negative charge on the working electrodes of the MEA. Power was supplied by either a direct current (DC) power source or a function generator (Keysight Technologies, CA, USA) for DC or CV release, respectively. We then filled each PDMS well with 300 µL of phosphate buffered saline (PBS), a pH neutral solution, to capture released quipazine. Depending on the experiment, films experienced an applied potential for 1 minute for DC release or 40 seconds for CV release. After each period, 100 µL of PBS was sampled from each well and

stored in an appropriately labeled vial. The remaining solution in each well was disposed of and then refilled with 300 µL of fresh PBS. All data depicted in this chapter is the summation of sample concentrations from discrete time points, unless otherwise noted.

4.2 UV-VIS SPECTROSCOPY

Quipazine concentrations were first detected using a UV-vis spectrometer (Spectramax i3). All readings were taken at 340 nm, selected based upon serial dilutions of quipazine in PBS (Figure 4.1). At 340 nm, samples exhibited a linear relationship between absorbance and concentration (R^2 > 0.99). We prepared quipazine standards, samples of PBS with known concentrations of drug, to create a linear relationship between concentration and absorbance. These standards were made by first weighing quipazine maleate, adding PBS, mixing thoroughly on a vortex, and sonicating for homogenization. For all experiments, a linear equation $y = mx$ was calculated based upon the absorbances, y, of known quipazine concentrations, x, in PBS. The absorbance of fresh PBS was subtracted from all experimental release samples to negate its influence.

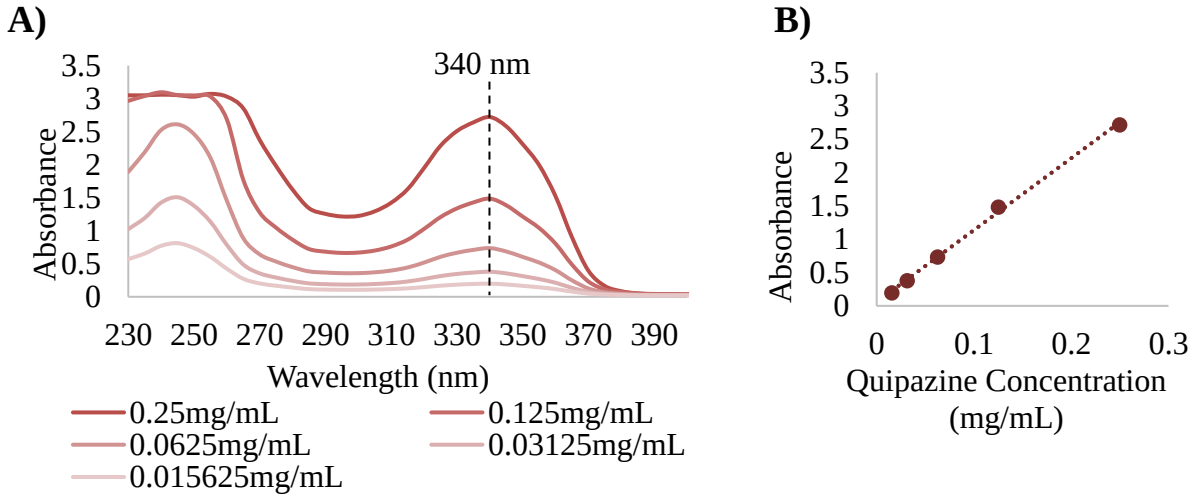

Figure 4.1 – Absorbance values obtained using UV-vis spectroscopy with known concentrations of quipazine dissolved in PBS (A) at wavelengths 230 to 390 nm, and (B) at the peak absorbance wavelength of 340 nm

4.2.1 *Experimental methods: Direct Current*

During initial testing of PPy-quipazine films, we looked at the influence of surfactant concentration on quipazine release. Films were divided into three experimental conditions based upon the bulk layer pyrrole solution: no quipazine (blank) with 0.2 M NaDBS, 1 mg/mL quipazine with no NaDBS, and 1 mg/mL quipazine with 0.2 M NaDBS. Regardless of the bulk layer type, all films contained an adhesion layer deposited with 0.2 M NaDBS at a charge density of 90 mC. The purpose for adding NaDBS to all conditions was to ensure film adhesion to the MEA; pyrrole solution without a chargeable dopant would not deposit on to the MEA. The bulk layers were deposited with a charge density of 240 mC for each of the three experimental film conditions. Films first were soaked in PBS for four minutes to allow for passive release. A volume of 200 µL was sampled from each well after the passing of one minute then stored into a UV transparent microplate. Controlled release trials were performed potentiostatically at 2 V and again sampled at 1-minute intervals. After each sample was taken, the chamber contents were removed and each well was refilled with PBS, as described in section 3.3.1.

4.2.2 *Results*

UV-vis spectroscopy could not accurately quantify quipazine released into PBS. As observed with blank films, there was evidence of overlapping spectra at 340 nm with other molecules in solution. Consequently, we could not decipher the release of quipazine from other products, most likely of which included free monomers or buffer solution ions [38]. If we assumed all release products to be quipazine, blank samples seemed to release quipazine after experiencing an applied voltage when compared to known absorbance values (Figure 4.2). Interestingly, both film types containing quipazine passively released compounds before the applied voltage, implying that the spontaneous release was likely influenced by the presence of quipazine.

Furthermore, the films with 0.2 M NaDBS and quipazine, immediately after controlled release began, had a dramatic increase in theoretical drug release and in variability. This result suggests that the surfactant likely played a role in more effectively depositing or releasing quipazine. However, since this data is fundamentally inflated, these results are strictly speculative, but have been included to emphasize the importance of selecting a quantification technique that is appropriately sensitive.

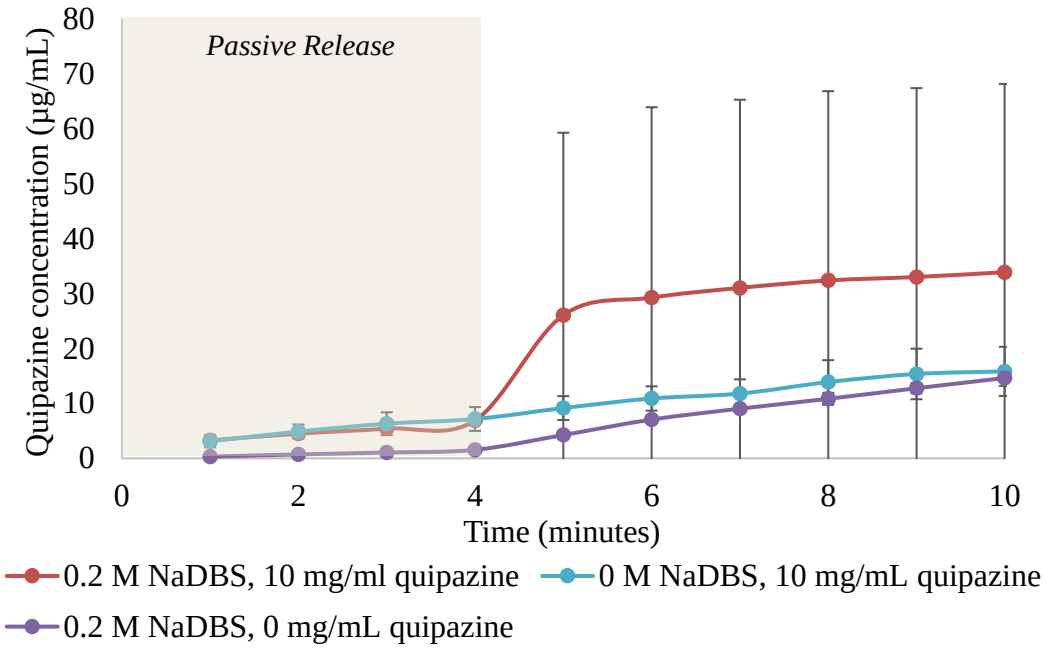

Figure 4.2 – Average quipazine release (n=4) with standard deviations as measured via UV-vis spectroscopy at 340 nm

4.3 Mass Spectrometry

In partnership with the Mass Spectrometry Center in the University of Washington School of Pharmacy, we developed a highly sensitive HPLC-QQQ method to quantify quipazine concentrations in PBS. The method utilized a reverse phase separation over a Waters C18 column (2.1 mm inner diameter, 100 mm in length) with a mobile phase composed of 10mM formic acid in water and 10mM formic acid in acetonitrile. A ballistic gradient was employed to rapidly change

the mobile phase composition. The analyte, quipazine maleate, was detected on a Xevo-XS triple quadrupole mass spectrometer.

4.3.1 *Implementing an internal standard*

Internal standards are used to ensure and track consistency of a sample from benchtop preparation to analysis. By adding the same amount of internal standard, a secondary analyte of interest, to every sample, we were able to track any changes that the sample may have been exposed to. This included the potential for any spillage, variable pipette volumes, autosampler issues, and loss in sensitivity on the mass spectrometer over time. Due to its relative availability and similar structure to quipazine maleate, we chose the compound MK-212 hydrochloride (Bio-Techne Corporation), hereafter denoted as MK-212. The daughter ion peak area of MK-212 was used to normalize all peak areas for quipazine; this was useful because the peak area ratios were linear with respect to quipazine concentration in solution. In subsequent analyses, all samples included 100 µL of MK-212 dissolved in PBS at a concentration of 0.25 µg/mL.

4.3.2 *Calculating quipazine concentrations*

To quantify quipazine released experimentally, we ran a series of samples with known quipazine concentrations ranging from 1.25 ng/mL to 10 µg/mL, referred to as calibration standards. For both the unknown samples and calibration standards, we spiked in the same amount of internal standard as described above. For both analytes, quipazine maleate and MK-212, we acquired two daughter ions. We then made a peak area ratio (PAR) for the best response of each. In our case, we used the daughter ion peak area of 128 *m/z* (for quipazine) over 93 *m/z* (for MK-212). The PAR for the calibration standards were plotted against known concentrations to create a linear equation, $y = mx + b$. The resulting equation was then applied to the PAR of unknown

samples from quipazine drug release experiments to return a concentration. An example calculation determining the concentration of an unknown experimental sample can be found in Appendix A. All calibration standards used to produce experimental results were linear ($R^2 > 0.99$).

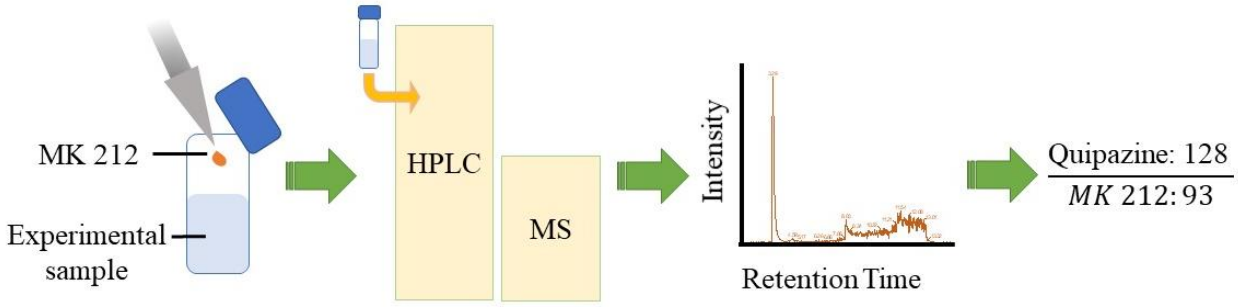

Figure 4.3 – Schematic of how data was extracted, starting from the spiking of MK-212, the internal standard, into the sample vial, the sample entering into the HPLC-MS system, producing a chromatogram, and then calculating the PAR

4.3.3 *Sample preparation and filtering*

Due to the potential buildup of free monomers on the chromatographic column, we chose to filter all experimental release samples. To understand the influence of filtering on experimental results, we analyzed ten different samples of quipazine maleate dissolved in PBS. Stock samples were prepared at concentrations ranging from 1 ng/mL to 10 µg/mL, encompassing the presumed range of unknown samples. We spiked two 100 µL samples of each concentration with MK- 212 (100 µL at 0.25 µg/mL). One sample at each concentration was set aside to establish the control group. The other sample at that concentration was drawn into a 1 mL syringe, then dispensed through an attachable, hydrophilic membrane with pore size 0.22 µm (Millipore Sigma).

The controlled, unfiltered group and the filtered group were analyzed using the HPLC-QQQ method. As expected, based on the size and type of the filter used, we did not observe a notable impact on sample concentrations. In a comparison of the expected to measured concentrations for the unfiltered and filtered samples, both conditions were linear ($R^2 > 0.99$)

(Figure 4.4). Additionally, the unfiltered and filtered samples produced slopes of 0.9840 and 0.9856, respectively, where a value of 1 would correspond to perfect accuracy.

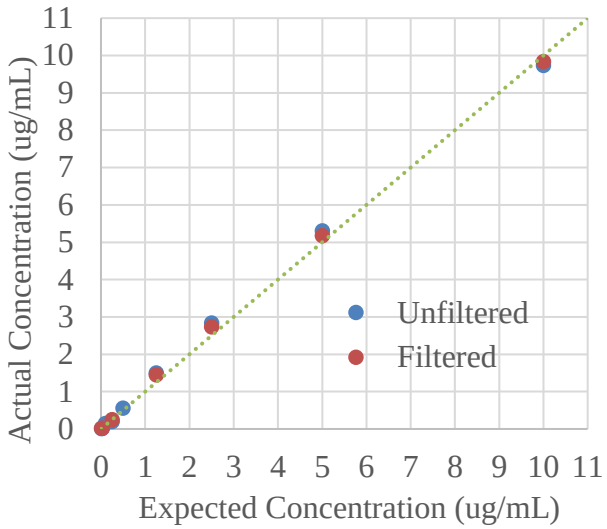

Figure 4.4 – Comparison of filtered and unfiltered samples with known quipazine concentrations plotted against a line demonstrating perfect return values (y = x)

4.3.4 *Proof-of-Concept Measurements of Released Quipazine*

Since UV-vis absorption spectroscopy could not return a true value of zero from films without quipazine, we needed to ensure that mass spectrometry would. Therefore, we repeated the DC release experiment with films at varying concentrations of NaDBS. Each of the 9 films (n=3 per arm) contained an adhesion layer produced from 0.2 M NaDBS pyrrole at a charge density of 90 mC. Bulk layers were deposited at 240 mC for the following three conditions of pyrrole stock: 0.02 M NaDBS with 5 mg/ml quipazine, 0.2 M NaDBS with 5 mg/ml quipazine, and 0.2 M NaDBS without quipazine. Films experienced a constant applied voltage of 2 V; samples were pulled every 30 seconds up to 150 seconds using standard procedures.

The first quipazine release experiment analyzed by the new HPLC-QQQ method met our expectations. Samples from all three PPy films lacking quipazine returned concentration values below the limit of detection for the mass spectrometer, which can be translated to a nominal value

of 0 µg/ml (Figure 4.5). As seen in Figure 4.2, the films with 0.2 M NaDBS released more quipazine cumulatively than their 0.02 M NaDBS counterparts over the duration of the experiment. However, we have more confidence in the release values produced by the HPLC-QQQ method due to the true zero returned and the consistency of sample measurements.

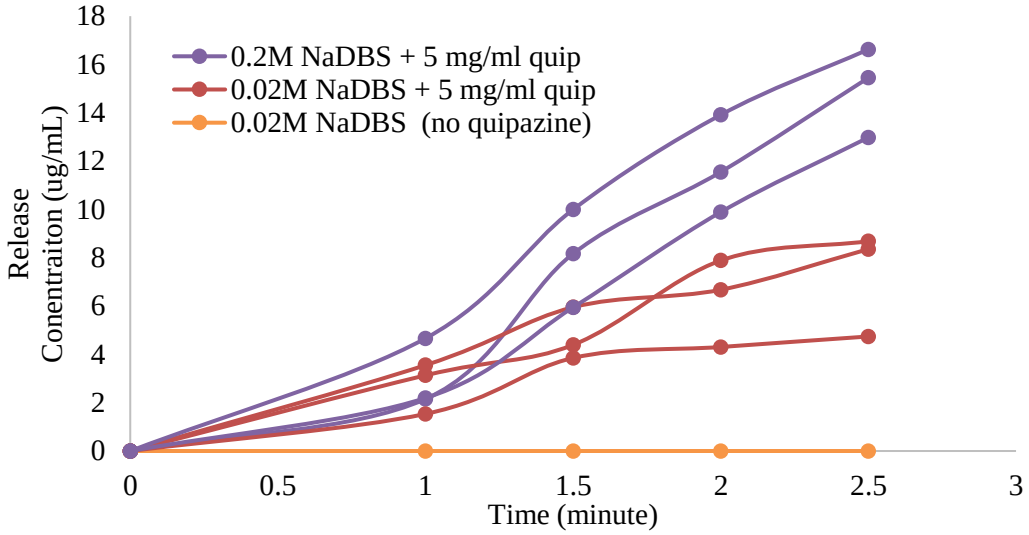

Figure 4.5 – Values of quipazine released using constant voltage from three conditions of PPy (n=3 each) into PBS as measured using the HPLC-QQQ method

4.3.5 *Experimental Methods: Cyclic Voltammetry*

To demonstrate MEA and chamber performance, we measured quipazine release from PPy films as triggered by CV. Films adhesion layers were deposited as previously described, at 90 mC. Bulk layers were deposited at 108 mC using a stock pyrrole solution of 10 mg/mL quipazine and 0.2 M NaDBS. Applied voltage alternated from -1 to +1 V at a scan rate of 100 mV/s. The experimental setup was verified using an oscilloscope (Siglent Technologies). Samples were taken from each MEA well after every full cycle, defined by the passing of 40 seconds, up to 15 full cycles equal to 600 seconds. The nine calibration samples were composed of PBS with quipazine concentrations ranging from 1.25 ng/mL to 10 µL.

4.3.6 *CV Results*

Release of quipazine from PPy films (n=8) climbed in cumulative concentrations up to approximately 10 CV cycles, where the upper limit of delivery was reached (Figure 4.6). After 15 CV cycles, average cumulative concentrations of quipazine with one standard deviation were 0.368 ± 0.108 µg/mL. The maximum concentration of quipazine delivered at a discrete time point was 0.149 ± 0.063 µg/mL, measured after 1 CV cycle. Qualitatively, the discrete release profile exponentially decays, similar to the release of a fluorescent particle from a composite PPy film [15], with one exception; after 7 CV cycles, the films universally had an increase in released concentrations. This behavior was unexpected and may indicate drug delivery mechanics requiring deeper exploration. Assuming perfect experimental and theoretical conditions, the films delivered a cumulative dosage of 220 ng quipazine (see Appendix A for calculations). Although there is no agreed upon therapeutic dosage of quipazine for delivery to the spinal cord, this experiment established a benchmark for future exploration of quipazine using the MEA and chamber.

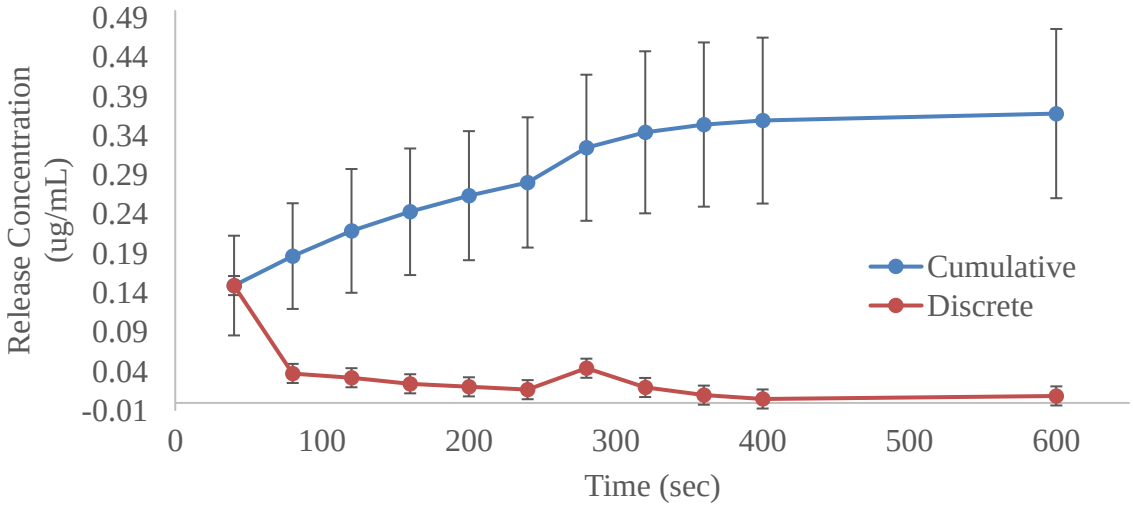

Figure 4.6 – Average concentrations of released quipazine from PPy films (108 mC deposition charge) triggered by cyclic voltammetry; equivalent data is depicted in two forms, by cumulative release (in blue) and by discrete release (in red) with appropriate standard deviations

From a design perspective, we wanted to investigate if film position on the MEA impacted drug release. Figure 4.7 depicts the same dataset as described above, with release profiles displayed for each film. Films were identified using numbers based upon positions relative to the positive power source terminal during deposition. Qualitatively, films had similar overall release profiles, a promising result regarding potential film variability. By observation, the first sample collected at 40 seconds seemed to be the differentiator for each film's net cumulative release. As more data is collected using the MEA and experimental platform, we will further investigate the impact of film location.

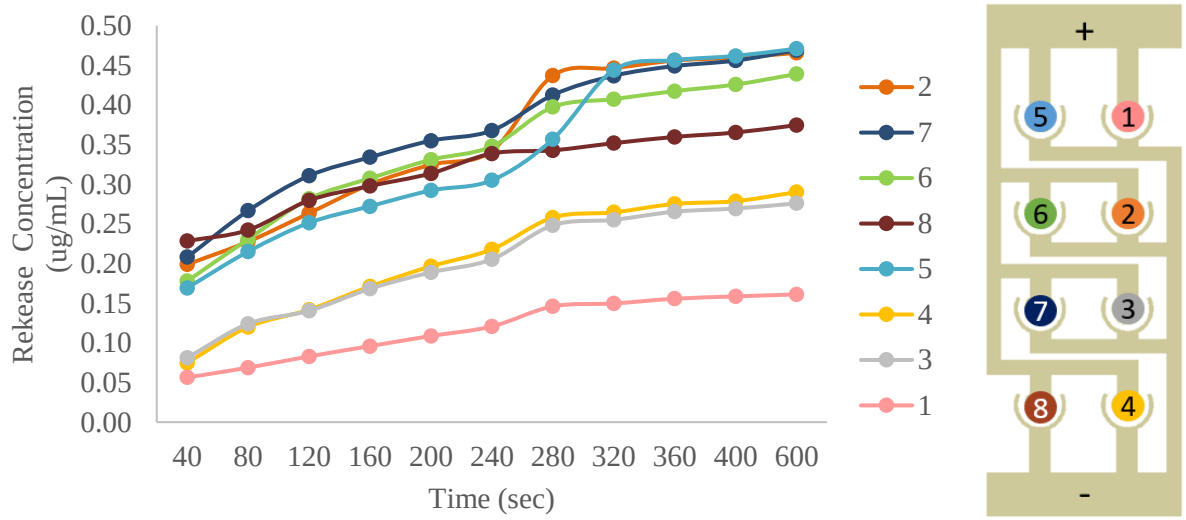

Figure 4.7 – Concentrations of released quipazine from eight PPy films (108 mC deposition charge) triggered by cyclic voltammetry and color-coded by position on the MEA relative to the applied potential during film deposition (labeled '+' for the positive and '-' for the negative terminals)

4.3.7 *Experimental Methods: Passive Release*

To investigate how PPy films behaved passively, or without an applied potential, we measured quipazine release over the course of six days. Like the CV protocol previously described, eight films were deposited at 56 mC using a stock pyrrole solution with 10 mg/mL quipazine. After

deposition, the power source was disconnected, each well was filled with 300 µL of PBS, and the experimental chamber was covered with tin foil to prevent evaporation. At 24, 48, 72, and 136 hours, 100 µL of sample was removed from each well and dispensed into eight individual tubes to be mixed with internal standard. After every sampling, the remaining PBS was removed, and each well was refilled with 300 µL PBS.

4.3.8 *Passive Release Results*

Quipazine was passively released from the PPy films for approximately 72 hours (Figure 4.8). After this time point, there were negligible changes in further quipazine release. From a design perspective, to achieve purely active control over quipazine, this data motivates a procedural change. One option for eliminating the passive release of quipazine is to pre-soak all films prior to experimental use for 3 days. Alternatively, we could implement a third layer on top of the existing two layers to prevent the movement of quipazine from the bulk. This so-called capping layer proved to be effective in limiting passive release for two model drugs released from PPy films on a microchip [14].

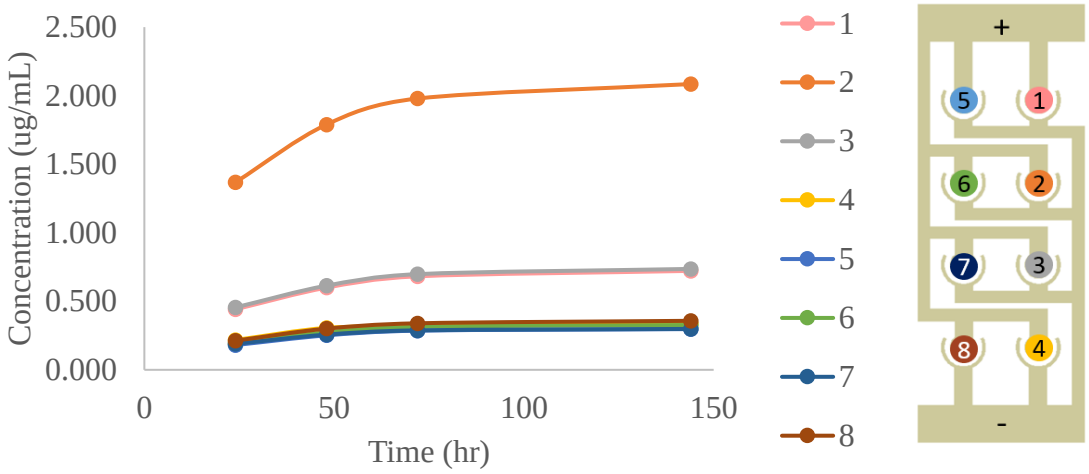

Figure 4.8 – Concentrations of passively released quipazine from eight PPy films (56 mC deposition charge), coded by position on the MEA relative to the applied potential during film deposition

Chapter 5. CONCLUSIONS AND FUTURE DIRECTIONS

In this paper, I have presented (i) the design and fabrication of a novel MEA, (ii) the integration of the MEA into an experimental chamber to deposit polypyrrole films, (iii) an HPLC-MS method to quantify quipazine in phosphate buffered saline, and (iv) preliminary measurements of quipazine released using the MEA. This platform has facilitated the first reported delivery of quipazine from thin films and will support future endeavors to tune the release of quipazine over time. Based upon the datasets presented in this thesis, the MEA does not appear to bias quipazine release results and functions as originally intended.

5.1 Future Directions

In partnership with the nanofabrication team at San Diego State University, advised by Dr. Sam Kassegne, we have proposed a design for the translation of PPy-quipazine films onto a flexible implant (Figure 5.1). This design, based upon prior work developing glassy-carbon electrodes [31], will allow for the deposition of up to 10 films. Each electrode site for these films can be independently controlled on a single channel to facilitate film deposition and quipazine release. An important next step to push forward this implant design will be to conduct preliminary *in vitro* studies, including impedance testing and proof-of-concept quipazine release experimentation. This implant will be implemented in an *in vivo* study of chronic SCI using a rodent model.

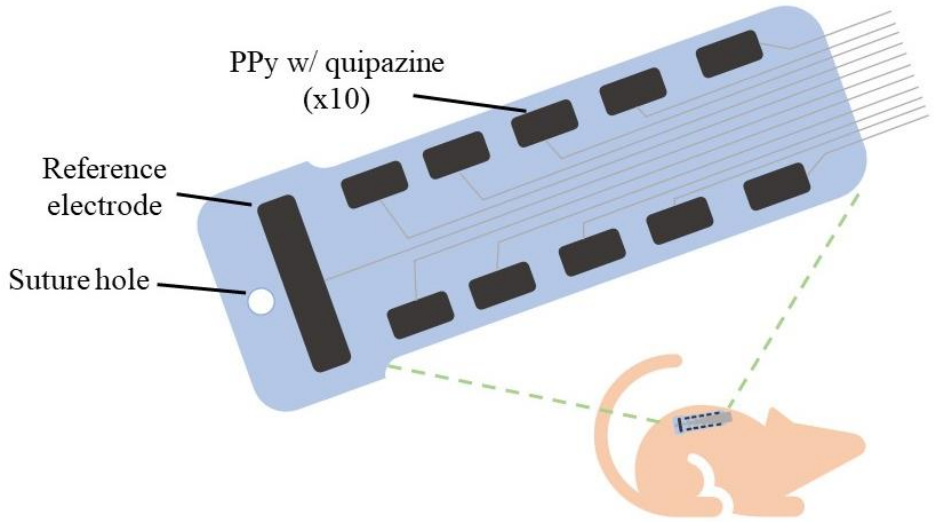

Figure 5.1 – Implantable device for local delivery of quipazine via PPy films

5.2 Closing Remarks

As a mechanical engineer tackling a problem deeply rooted in bioengineering, physics, and material science, this thesis reinforced the importance of thinking critically and involving multidisciplinary perspectives. Ultimately, the MEA platform has and will continue to be leveraged to study quipazine release and understand variability. Assuring repeatability under similar manufacturing and stimulation paradigms will be the key to translating targeted quipazine delivery in animal models.

REFERENCES

1. Maton, A., *Human Biology and Health*. 1993: Englewood Cliffs, N.J. : Prentice Hall.

2. Alizadeh, A., S.M. Dyck, and S. Karimi-Abdolrezaee, *Traumatic Spinal Cord Injury: An Overview of Pathophysiology, Models and Acute Injury Mechanisms.* Front Neurol, 2019. **10**: p. 282.

3. Jain, N.B., et al., *Traumatic spinal cord injury in the United States, 1993-2012.* JAMA, 2015. **313**(22): p. 2236-43.

4. Angeli, C.A., et al., *Recovery of Over-Ground Walking after Chronic Motor Complete Spinal Cord Injury.* N Engl J Med, 2018. **379**(13): p. 1244-1250.

5. Gill, M.L., et al., *Neuromodulation of lumbosacral spinal networks enables independent stepping after complete paraplegia.* Nat Med, 2018. **24**(11): p. 1677-1682.

6. Rejc, E., C. Angeli, and S. Harkema, *Effects of Lumbosacral Spinal Cord Epidural Stimulation for Standing after Chronic Complete Paralysis in Humans.* PLoS One, 2015. **10**(7): p. e0133998.

7. Minev, I.R., et al., *Electronic dura mater for long-term multimodal neural interfaces.* Science, 2015. **347**(6218): p. 159-163.

8. Gerasimenko, Y.P., et al., *Epidural Spinal Cord Stimulation Plus Quipazine Administration Enable Stepping in Complete Spinal Adult Rats.* J Neurophysiol, 2007. **98**(5): p. 2525-36.

9. Fong, A.J., et al., *Spinal Cord-Transected Mice Learn to Step in Response to Quipazine Treatment and Robotic Training.* J Neurosci, 2005. **25**(50): p. 11738-47.

10. Asboth, L., et al., *Cortico-reticulo-spinal circuit reorganization enables functional recovery after severe spinal cord contusion.* Nat Neurosci, 2018. **21**(4): p. 576-588.

11. Kyosti Kontturi, P.P., Goran Sundholm, *Polypyrrole as a model membrane for drug delivery.* Journal of Electroanalytical Chemistry, 1998. **453**(1-2): p. 231-238.

12. George, P.M., et al., *Electrically Controlled Drug Delivery from Biotin-Doped Conductive Polypyrrole.* Advanced Materials, 2006. **18**(5): p. 577-581.

13. Nishizawa, M., et al., *Electrodeposition of anchored polypyrrole film on microelectrodes and stimulation of cultured cardiac myocytes.* Biomaterials, 2007. **28**(8): p. 1480-5.

14. Ge, D., et al., *A polypyrrole-based microchip for controlled drug release.* Electrochimica Acta, 2009. **55**(1): p. 271-275.

15. Du, Z.J., G.-Q. Bi, and X.T. Cui, *Electrically Controlled Neurochemical Release from Dual-Layer Conducting Polymer Films for Precise Modulation of Neural Network Activity in Rat Barrel Cortex.* Advanced Functional Materials, 2018. **28**(12).

16. Leprince, L., et al., *Dexamethasone electrically controlled release from polypyrrole-coated nanostructured electrodes.* J Mater Sci Mater Med, 2010. **21**(3): p. 925-30.

17. Wadhwa, R., C.F. Lagenaur, and X.T. Cui, *Electrochemically controlled release of dexamethasone from conducting polymer polypyrrole coated electrode.* J Control Release, 2006. **110**(3): p. 531-41.

18. George, P.M., et al., *Three-dimensional conductive constructs for nerve regeneration.* J Biomed Mater Res A, 2009. **91**(2): p. 519-27.

19. Gao, W. and R.B. Borgens, *Remote-controlled eradication of astrogliosis in spinal cord injury via electromagnetically-induced dexamethasone release from "smart" nanowires.* J Control Release, 2015. **211**: p. 22-7.

20. Hawryluk, G., et al., *Mean Arterial Blood Pressure Correlates with Neurological Recovery after Human Spinal Cord Injury: Analysis of High Frequency Physiologic Data.* J Neurotrauma, 2015. **32**(24): p. 1958-67.

21. Orr, M.B. and J.C. Gensel, *Spinal Cord Injury Scarring and Inflammation: Therapies Targeting Glialand Inflammatory Responses.* Neurotherapeutics, 2018. **15**(3): p. 541-553.

22. Bracken, M.B., et al., *Administration of methylprednisolone for 24 or 48 hours or tirilazad mesylate for 48 hours in the treatment of acute spinal cord injury. Results of the Third National Acute Spinal Cord Injury Randomized Controlled Trial. National Acute Spinal Cord Injury Study.* JAMA, 1997. **277**(20): p. 1597-604.

23. Gao, W., et al., *Action at a distance: functional drug delivery using electromagnetic-field-responsive polypyrrole nanowires.* Langmuir, 2014. **30**(26): p. 7778-88.

24. Koch, B., et al., *Microfabrication for Drug Delivery.* Materials (Basel), 2016. **9**(8).

25. Langer, R., *New methods of drug delivery.* Science, 1990. **249**(4976): p. 1527-1533.

26. Boehler, C., F. Oberueber, and M. Asplund, *Tuning drug delivery from conducting polymer films for accurately controlled release of charged molecules.* J Control Release, 2019. **304**: p. 173-180.

27. *Professor Robert S. Langer*. [cited 2019; Available from: langerlab.mit.edu/langer-bio/.

28. John T Santini, M.J.C., Robert Langer, *A controlled-release microchip.* Nature, 1999. **397**(6717): p. 335-8.

29. Onanuga, T., M. Rumler, and A. Erdmann. *A physical model for innovative laser direct write lithography*. in *SPIE Advanced Lithography*. 2017. San Jose, CA.

30. Bishop, C.A., *Electron Beam (E-beam) Evaporation,* in *Vacuum Deposition onto Webs, Films and Foils (Second Edition)*. 2011, William Andrew. p. 261-272.

31. Vomero, M., et al., *A novel pattern transfer technique for mounting glassy carbon microelectrodes on polymeric flexible substrates.* Journal of Micromechanics and Microengineering, 2016. **26**(2).

32. Vomero, M., et al., *Highly Stable Glassy Carbon Interfaces for Long-Term Neural Stimulation and Low-Noise Recording of Brain Activity.* Sci Rep, 2017. **7**: p. 40332.

33. Salas, M., M. Cervantes, and C. Guzman-Flores, *Mechanism of action of quipazine maleate on the central nervous system.* Boletín del Instituto de Estudios Médicos y Biológicos, 1966. **24**(1): p. 191-205.

34. Eidelberg, E., et al., *Stepping by chronic spinal cats.* Exp Brain Res, 1980. **40**(3): p. 241-6.

35. Landry, E.S. and P.A. Guertin, *Differential effects of 5-HT1 and 5-HT2 receptor agonists on hindlimb movements in paraplegic mice.* Prog Neuropsychopharmacol Biol Psychiatry, 2004. **28**(6): p. 1053-60.

36. Vicente-Torres, M.A., et al., *Simultaneous HPLC quantification of monoamines and metabolites in the blood-free rat cochlea.* Journal of Neuroscience Methods, 2002. **119**(1): p. 31-36.

37. Worsfold, P.J. and E.A.G. Zagatto, *Spectrophotomotry | Overview*, in *Encyclopedia of Analytical Science*. 2019. p. 244-248.

38. Boehler, C. and M. Asplund, *A detailed insight into drug delivery from PEDOT based on analytical methods: Effects and side effects.* J Biomed Mater Res A, 2014. **103**(3): p. 1200-7.

39. Santini, J.T., Jr., M.J. Cima, and R. Langer, *A controlled-release microchip.* Nature, 1999. **397**(28): p. 335-338.

40. Maia, G., et al., *Charge Compensation Dynamics in the Redox Processes of Polypyrrole-Modified Electrodes.* The Journal of Physical Chemistry, 1996. **100**(39): p. 15910-15916.

41. Sirivisoot, S., R. Pareta, and T.J. Webster, *Electrically controlled drug release from nanostructured polypyrrole coated on titanium.* Nanotechnology, 2011. **22**(8): p. 085101.

42. Svirskis, D., et al., *Evaluation of physical properties and performance over time of an actuating polypyrrole based drug delivery system.* Sensors and Actuators B: Chemical, 2010. **151**(1): p. 97-102.

43. Saigal, R., *Conductive Polymers for Controlled Release and Treatment of Central Nervous System Injury*, in *Engineering Sciences*. 2009, Harvard University: ProQuest Dissertations And Theses.

44. Priano, G., et al., *Disposable Gold Electrode Array for Simultaneous Electrochemical Studies.* Electroanalysis, 2008. **20**(1): p. 91-97.

45. Auner, A.W., et al., *Chemical-PDMS binding kinetics and implications for bioavailability in microfluidic devices.* Lab Chip, 2019. **19**(5): p. 864-874.

46. Nemani, K.V., et al., *In vitro and in vivo evaluation of SU-8 biocompatibility.* Mater Sci Eng C Mater Biol Appl, 2013. **33**(7): p. 4453-9.

47. Teh, K.S., et al., *Influence of redox-induced restructuring of polypyrrole on its surface morphology and wettability.* Sensors and Actuators A: Physical, 2009. **155**(1): p. 113-119.

APPENDIX A

Section 4.3.2: Example calculation

1. *Given peak areas for four daughter ions from an unknown experimental release sample:*

Quipazine:145	Quipazine:128	MK-212:113	MK-212:93
1631467	9033592	31841548	24526980

2. *The linear fit from calibration standards to relate the peak area ratio to quipazine concentration:*

$$y = 0.229873326x + 0.053824569$$

3. *Solve for the unknown concentration using known function:*

$$\text{concentration} = \frac{\text{Quipazine: 128}}{\text{MK 212: 93}} - \text{intercept} \Big/ \text{slope} = \frac{9033592}{24526980} - 0.053824569 \Big/ 0.229873326$$

$$= \mathbf{1.368\ \mu g/mL}$$

Section 4.3.6: Total quipazine delivery calculation

Assuming homogeneous concentrations of quipazine are released into each well from the MEA, and that 100 µL samples are representative of the homogeneous solution:

- 0.368 µg/mL = the average quipazine concentration measured by the HPLC-QQQ method after 15 CV cycles
- 0.736 µg/ml = 2 x 0.368 µg/mL = the theoretical average quipazine concentration sampled, since each sample is diluted by half with the addition of µL of PBS containing the internal standard
- ~220 ng = 0.736 µg/ml x 0.300 ml = the total amount of quipazine delivered in each well containing 300 µl of PBS